

Image-based surface reconstruction in geomorphometry – merits, limits and
developments

A. Eltner, A. Kaiser, C. Castillo, G. Rock, F. Neugirg, and A. Abellan

Associate Editor Decision: Publish subject to minor revisions (review by Editor)
(25 Apr 2016) by Dr. Giulia Sofia

Comments to the Author:

Dear Authors, your revised work has now been considered by the two reviewers. They both agree that a significant effort was done and the paper is now improved significantly. The manuscript is now more readable, and its structure is much more clear, with a clear highlight and description of the main objectives of the manuscript throughout the text.

One of the reviewers wonders if the sections about errors should be combined into a single one, rather than be separated. Otherwise, the only other point of concern the reviewer has is about the standard of written English, that might need some improvement throughout. Some additional comments are attached.

I believe that at this stage, the manuscript provides a valid asset to researchers dealing with the SfM method. However, a further minor revision is required: the revised version of the manuscript will be reviewed at the editorial level before acceptance. Please during the review, make sure to provide a proper rebuttal to the reviewer's comments, and highlight the corresponding changes in the manuscript.

Please note that this re-submission does not ensure a final publication in ESurf: a decision will be made only when the revised version will be evaluated carefully. Thank you for submitting to the Special Issue, and I look forward to receiving the revised manuscript.

Kind Regards

Giulia Sofia

Thank you, Giulia Sofia, for the handling of our manuscript. We are very grateful for your time and advices.

We add a file containing the changes we made to the manuscript (changes tracked).

We further proofread the article regarding the English standard.

Non-public comments to the Author:

Additional comments from Reviewer #2

I am generally satisfied that Eltner and co-authors have addressed the majority of concerns raised by myself and another reviewer in their revised manuscript. I have a number of minor points to raise, which are listed below.

General comment – the standard of written English needs some work throughout. In places it can detract from the flow of the article – I would suggest further proofreading to improve if possible.

48 *We would like to thank Matt Westoby for his great support and the time he spent to*
49 *evaluate our manuscript. We are very grateful for his comments that again improved the*
50 *article.*

51

52 L31 – add a reference here to Lowe’s SIFT work

53 - *Thank you for the remark. However, we would like to keep this statement general*
54 *because it is unusual to cite in abstracts. However, we added the corresponding*
55 *reference in the main text later on.*

56

57 L47 – any references to support this?

58 - *We added a reference in the text and the reference list.*

59

60 L51 – how is it driven by digital sensors? What aspects of these technologies? Cost? Ease
61 of use? Please be more specific for the reader.

62 - *The issue has been clarified more specifically.*

63

64 L69 – you don’t mention here the range of temporal or spatial scales that can be
65 captured and I think that you need to. The wording is quite vague. It would help to put
66 numbers to these scales – e.g. millimetric to kilometric for spatial scale, and, I suppose,
67 survey visit scales of minutes or pretty much any interval longer than this?

68 - *We added numbers to the temporal and spatial scale statement.*

69

70 L94 – remove ‘great’ – suggest replace with ‘valuable’, or similar.

71 - *Done.*

72

73 L149 – typo for Helmert transformation

74 - *Corrected*

75

76 L199 – what does ‘APERO’ do? Please describe very briefly at the end of this sentence.
77 Ah, you mention this at L217 – perhaps shift this text earlier to match first usage.

78 - *We clarified APERO with a sub-clause.*

79

80 L225 – you could just name this section ‘Key developments in SfM photogrammetry’

81 - *Done.*

82

83 Sections 3 and 4 – Whilst the authors have taken on board the reviewers’ comments and
84 have performed some restructuring of the manuscript, more could be done to improve it
85 further. For example, I do not understand why the content of section 3.2 and section 5
86 appear in different sections. At present, the authors talk about error analysis in section
87 3.2, then describe the various applications of SfM by sub-discipline, and then return to
88 error analysis again in section 5. This is very confusing and does not flow well. The
89 text/discussion for both of these ‘error analysis’ sections needs combining, and should
90 come after current section 4 – i.e. integrate the text from section 3.2 into section 5.

91 - *We restructured the manuscript accordingly.*

92
93 L447 – these sub-sub-sections need numbering as well as per the ESD manuscript
94 formatting guidelines.
95 - *Thank you. We corrected it.*
96
97 L784 – this paragraph/section is very, very short – I would request that the authors
98 either expand this section or integrate the text into another section as appropriate.
99 - *We integrated the paragraph into chapter 5.5*
100
101 L792 – exactly how has the development of open-source software (e.g. CloudCompare)
102 ‘boosted’ geomorphometric studies? Please be more specific – do you mean because
103 these types of software can easily handle massive datasets containing tens of millions of
104 points (or more?), whereas this has been an obstacle for researchers previously?
105 - *We added a sub-clause for further explanation.*
106
107 L805 – should be ‘Google Street View’
108 - *Corrected.*
109

Image-based surface reconstruction in geomorphometry – merits, limits and developments

A. Eltner¹, A. Kaiser², C. Castillo³, G. Rock⁴, F. Neugirg⁵ and A. Abellan⁶

[1] {Institute of Photogrammetry and Remote Sensing, Technical University Dresden, Germany}

[2] {Soil and Water Conservation Unit, Technical University Freiberg, Germany}

[3] {Dep. of Rural Engineering, University of Córdoba, Spain}

[4] {Dep. of Environmental Remote Sensing and Geomatics, University of Trier, Germany}

[5] {Dep. of Physical Geography, Catholic University Eichstätt-Ingolstadt, Germany}

[6] {Risk Analysis Group, Institute of Earth Sciences, University of Lausanne, Switzerland}

Correspondence to: A. Eltner (Anette.Eltner@tu-dresden.de)

Abstract

Photogrammetry and geosciences have been closely linked since the late 19th century due to the acquisition of high-quality 3D datasets of the environment, but it has so far been restricted to a limited range of remote sensing specialists because of the considerable cost of metric systems for the acquisition and treatment of airborne imagery; Nowadays, a wide range of commercial and open-source software tools enable the generation of 3D and 4D models of complex geomorphological features by geoscientists and other non-experts users. In addition, very recent rapid developments in unmanned aerial vehicle (UAV) technology allows for the flexible generation of high quality aerial surveying and orthophotography at a relatively low-cost.

The increasing computing capabilities during the last decade, together with the development of high-performance digital sensors and the important software innovations developed by computer based vision and visual perception research fields has extended the rigorous processing of stereoscopic image data to a 3D point cloud generation from a series of non-calibrated images. Structure from motion (SfM) workflows are based upon algorithms for efficient and automatic orientation of large image sets without further data acquisition information, examples including robust feature detectors like the scale-invariant feature transform for 2D-imagery. Nevertheless, the importance of carrying out well-established

fieldwork strategies, using proper camera settings, ground control points and ground truth for understanding the different sources of errors still need to be adapted in the common scientific practice.

This review intends not only to summarize the current state of the art on using SfM workflows in geomorphometry, but also to give an overview of terms and fields of application. Further this article aims to quantify already achieved accuracies and used scales using different strategies, to evaluate possible stagnations of current developments and to identify key future challenges. It is our belief that some lessons learned in already published articles, scientific reports and book chapters concerning the identification of common errors or “bad practices” and some other valuable information may help in guiding the future use of SfM photogrammetry in geosciences.

1 Introduction

Early works on projective geometries date back to more than five centuries, when scientists derived coordinates of points from several images and investigated the geometry of perspectives (Doyle, 1964). Projective geometry represents the basis for the developments in photogrammetry in the late 19th century, when Aimé Laussedat experimented with terrestrial imagery as well as kites and balloons for obtaining imagery for topographic mapping (Laussedat, 1899). Rapidly, photogrammetry advanced to be an essential tool in geosciences during the last two decades and is lately gaining momentum driven by digital sensors leading to flexible, fast and facile generation of images. Simultaneously, growing computing capacities and rapid developments in computer vision led to the method of Structure from Motion (SfM) that opened the way for low-cost high-resolution topography. Thus, the community using image-based 3D reconstruction experienced a considerable growth, not only in quality and detail of the achieved results but also in the number of potential users from diverse geo-scientific disciplines.

SfM photogrammetry can be performed with images acquired with consumer grade digital cameras and is thus very flexible in its implementation. Its ease of use in regard to data acquisition and processing makes it further interesting to non-experts (Fig. 1). The diversity of possible applications led to a variety of terms used to describe SfM photogrammetry either from photogrammetric or computer vision standpoint. Thus to avoid ambiguous terminology, a short list of definitions in regard to the reviewed method is given in Table 1. In this review a series of studies that utilise the algorithmic advance of high automatisation in SfM are

considered, i.e. no initial estimates of the image network geometry or user interactions to generate initial estimates are needed. Furthermore, data processing can be performed almost fully automatic. However, some parameter settings, typical for photogrammetric tools (e.g. camera calibration values), can be applied to optimise both accuracy and precision, and GCP or scale identification are still necessary.

SfM photogrammetry can be applied to a vast range of temporal scales (reaching from sub-seconds to decades) as well as spatial scales (reaching from sub-millimetres to kilometres) and resolutions up to an unprecedented level of detail, allowing for new insights into earth surface processes, i.e. 4D (three spatial dimensions and one temporal dimension) reconstruction of environmental dynamics. For instance, the concept of sediment connectivity (Bracken et al., 2014) can be approached from a new perspective through varying spatio-temporal scales. Thereby, the magnitude and frequency of events and their interaction can also be evaluated. Furthermore, the versatility of SfM photogrammetry utilising images captured from aerial or terrestrial perspectives has the advantage of being applicable in remote areas with limited access and in fragile, fast changing environments.

After the suitability of SfM has been noticed for geo-scientific applications (James and Robson, 2012, Westoby et al., 2012, Fonstad et al., 2013) the number of studies utilising SfM photogrammetry for geomorphometric investigations (thereby referring to the “science of topographic quantification” after Pike et al., 2008) has increased significantly. However, the method needs sophisticated study design and some experience in image acquisition to prevent predictable errors and to ensure good quality of the reconstructed scene. Smith et al. (2015) and Micheletti et al. (2015) recommend a setup for efficient data acquisition.

A total of 65 publications are reviewed in this study. They are chosen according to the respective field of research and methodology. Only studies are included that make use of the benefits of automatic image matching algorithms and thus apply the various SfM tools. Studies that lack of full automatisation are excluded, i.e. some traditional photogrammetric software. Topic wise a line is drawn in regard to the term geosciences. The largest fraction of the reviewed articles tackles questions arising in geomorphological contexts. To account for the versatility of SfM photogrammetry, a few studies deal with plant growth on different scales (moss, crops, forest) or investigate rather exotic topics such as stalagmites or reef morphology.

This review aims to highlight the development of SfM photogrammetry as a great-valuable tool for geoscientists:

- (1) The method of SfM photogrammetry is briefly summarised and algorithmic differences due to their emergence from computer vision as well as photogrammetry are clarified (section 2).
- (2) Open-source tools regarding SfM photogrammetry are introduced as well as beneficial tools for data post-processing (section 3).
- (3) Different fields of applications where SfM photogrammetry led to new perceptions in geomorphometry are displayed (section 4).
- (4) The performance of the reviewed method is evaluated (section 5).
- (5) And frontiers and significance of SfM photogrammetry are discussed (section 6).

2 SfM photogrammetry: method outline

2.1 Basic concept

Reconstruction of three-dimensional geometries from images has played an important role in the past centuries (Ducher, 1987, Collier, 2002). The production of high-resolution DEMs was and still is one of the main applications of (digital) photogrammetry. Software and hardware developments as well as the increase in computing power in the 1990s and early 2000s made aerial photogrammetric processing of large image datasets accessible to a wider community (e.g. Chandler, 1999).

Camera orientations and positions, which are usually unknown during image acquisition, have to be reconstructed to model a 3D scene. For that purpose, photogrammetry has developed bundle adjustment (BA) techniques, which allowed for simultaneous determination of camera orientation and position parameters as well as 3D object point coordinates for a large number of images (e.g. Triggs et al, 2000). The input into the BA are image coordinates of many tie points. If the BA is extended by a simultaneous calibration option, even the intrinsic camera parameters can be determined in addition to the extrinsic parameters. Furthermore, a series of ground control points can be used as input into BA for geo-referencing the image block (e.g. Luhmann et al., 2014, Kraus, 2007, Mikhail et al., 2001).

Parallel developments in computer vision took place that try to reconstruct viewing geometries of image datasets not fulfilling the common prerequisites from digital photogrammetry, i.e. calibrated cameras and initial estimates of the image acquisition scheme. This led to the SfM technique (Ullman, 1979) allowing to process large datasets and to use a combination of multiple non-metric cameras.

The typical workflow of SfM photogrammetry (e.g. Snavely et al., 2008) comprises the following steps:

- (1) identification and matching of homologous image points in overlapping photos (image matching, e.g. Lowe, 1999),
- (2) reconstruction of the geometric image acquisition configuration and of the corresponding 3D coordinates of matched image points (sparse point cloud) with iterative BA,
- (3) dense matching of the sparse point cloud from reconstructed image network geometry,
- (4) scaling or geo-referencing, which is also performable within step 2.

Smith et al. (2015) give a detailed description of the workflow of SfM photogrammetry, especially regarding step 1 and step 2.

In contrast to classical photogrammetry software tools, SfM allows for reliable processing of a large number of images in rather irregular image acquisition schemes (Snavely et al., 2008) with a much higher degree of process automation. Thus, one of the main differences between usual photogrammetric workflow and SfM is the emphasis on either accuracy or automation, with SfM focusing on the latter (Pierrot-Deseilligny and Clery, 2011). Another deviation between both 3D reconstruction methods is the consideration of GCPs (James and Robson, 2014, Eltner and Schneider, 2015). Photogrammetry performs BA either one-staged, considering GCPs within the BA, or two-staged, performing geo-referencing after a relative image network configuration has been estimated (Kraus, 2007). In contrast, SfM is solely performed in the manner of a two-staged BA concentrating on the relative orientation in an arbitrary coordinate system. Thus, absolute orientation has to be conducted separately with a seven parameter 3D-Helmert-transformation, i.e. three shifts, three rotations and one scale. This can be done, for instance, with the freeware tool *sfm-georef* that also gives accuracy information (James and Robson, 2012). Using GCPs has been proven to be relevant for specific geometric image network configurations, as parallel-axes image orientations usual for UAV data, because adverse error propagation can occur due to unfavourable parameter correlation, e.g. resulting in the non-linear error of a DEM dome (Wu, 2014, James and Robson, 2014, Eltner and Schneider, 2015). Within a one-staged BA these errors are minimised because during the adjustment calculation additional information from GCPs is employed, which is not possible, when relative and absolute orientation are not conducted in one stage.

The resulting oriented image block allows for a subsequent dense matching, measuring many more surface points through spatial intersection to generate a DEM with very high resolution.

Recent developments in dense matching allow for resolving object coordinates for almost every pixel. To estimate 3D coordinates, pixel values are either compared in image-space in the case of stereo-matching, considering two images, or in the object space in the case of MVS-matching, considering more than two images (Remondino et al., 2014). Furthermore, local or global optimisation functions (Brown et al., 2003) are considered, e.g. to handle ambiguities and occlusion effects between compared pixels (e.g. Pears et al., 2012). To optimise pixel matching, (semi-)global constraints consider the entire image or image scan-lines (e.g. semi-global matching (SGM) after Hirschmüller, 2011), whereas local constraints consider a small area in direct vicinity of the pixel of interest (Remondino et al., 2014).

SfM photogrammetry software packages are available partially as freeware or even open-source. Most of the packages comprise SfM techniques in order to derive 3D reconstructions from any collection of unordered photographs, without the need of providing camera calibration parameters and high accuracy ground control points. As a consequence, no in-depth knowledge in photogrammetric image processing is required in order to reconstruct geometries from overlapping image collections (James and Robson, 2012, Westoby et al., 2012, Fonstad et al., 2013). But now, also many photogrammetric tools utilise abilities from SfM to derive initial estimates automatically (i.e. automation) and then perform photogrammetric BA with the possibility to set weights of parameters for accurate reconstruction performance (i.e. accuracy). In this review studies are considered, which either use straight SfM tools from computer vision or photogrammetric tools implementing SfM algorithms that entail no need for initial estimates in any regard.

2.2 Tools for SfM photogrammetry and data post processing

SfM methodologies rely inherently on automated processing tools which can be provided by different non-commercial or commercial software packages. Within the commercial approach PhotoScan (Agisoft LLC, Russia), Pix4D (Pix4D SA, Switzerland) and MENCİ APS (MENCİ Software, Italy) represent complete solutions for 3D photogrammetric processing that have been used in several of the reviewed works.

Initiatives based on non-commercial software have played a significant role in the development of SfM photogrammetry approaches, either 1) open-source, meaning the source code is available with a license for modification and distribution; 2) freely-available, meaning the tool is free to use but no source code is provided or 3) under free web service with no access to the code, intermediate results or possible secondary data usage (Table 2). The

pioneer works by Snavely et al. (2006, 2008) and Furukawa and Ponce (2010) as well as Furukawa et al. (2010) provided the basis to implement one of the first open-source workflows for free SfM photogrammetry combining Bundler and PMVS2/CMVS as in SfMToolkit (Astre, 2015). By 2007, the MicMac project, which is open-source software originally developed for aerial image matching, became available to the public and later evolved to a comprehensive SfM photogrammetry pipeline with further tools such as APERO [to estimate image orientation](#) (Pierrot-Deseilligny and Clery, 2011).

Further contributors put their efforts in offering freely-available solutions based on Graphical User Interfaces (GUI) for SfM photogrammetry (VisualSfM by Wu, 2013) and geo-referencing (sfm_georef by James and Robson, 2012). The need for editing large point-cloud entities from 3D reconstruction led to the development of open-source specific tools such as Meshlab (Cignoni et al., 2008) or CloudCompare (Girardeau-Montaut, 2015), also implementing GUIs. Sf3M (Castillo et al., 2015) exploits VisualSfM and sfm_georef and additional CloudCompare command-line capacities for image-based surface reconstruction and subsequent point cloud editing within one GUI tool. Overall, non-commercial applications have provided a wide range of SfM photogrammetry related solutions that are constantly being improved on the basis of collaborative efforts. Commercial software packages are not further displayed due to their usual lack of detailed information regarding applied algorithms and their black box approach.

A variety of tools of SfM photogrammetry (at least 10 different) are used within the differing studies of this review (Fig. 3). Agisoft PhotoScan is by far the most employed software, which is probably due to its ease of use. However, this software is commercial and works after the black box principle, which is in contrast to the second most popular tools Bundler in combination with PMVS or CMVS. The tool APERO in combination with MicMac focuses on accuracy instead of automation (Pierrot-Deseilligny and Clery, 2011), which is different to the former two. The high degree of possible user-software interaction that can be very advantageous to adopt the 3D reconstruction to each specific case study might also be its drawback because further knowledge into the method is required. Only a few studies have used the software in geo-scientific investigations (Bretar, et al., 2013, Stumpf et al., 2014, Ouédraogo et al., 2014, Stöcker et al., 2015, Eltner and Schneider, 2015).

3 Approaches to identify key developments of in SfM photogrammetry

The vast recognition of SfM photogrammetry resulted in a large variety of its implementation leading to methodological developments, which have validity beyond its original application. Thus regarding geomorphometric investigations, studies considering field of applications as well as evaluations of the method performance induced key advances for SfM photogrammetry to establish as a standard tool in geosciences (Table 3). In the following, the approaches are introduced concerning the selection and retrieval of scientific papers utilising SfM photogrammetry. ~~and methods illustrated concerning integrated consideration of error performance of SfM photogrammetry in geo-scientific studies.~~

3.1 Selection of scientific papers exploiting SfM photogrammetry

A survey of 65 scientific papers published between 2012 and 2015 was conducted, covering a wide range of applications of SfM photogrammetry in geo-scientific analysis (see Appendix A for a detailed list). Common scientific journals, academic databases and standard online searches have been used to search for corresponding publications. Although, it has to be noted that our approach does not guarantee full coverage of the published works using SfM photogrammetry in geosciences. Nevertheless, various disciplines, locations and approaches from all continents are contained in this review (Fig. 2).

To put research hot spots in perspective it should be taken into account that the amount of publications in each discipline is not only dependent on the applicability of the method in that specific field of research. To a greater degree it is closely linked to the overall number of studies, which in the end can probably be broken down to the actual amount of researchers in that branch of science. Relative figures revealing the relation between SfM photogrammetry oriented studies to all studies of a given field of research would be desirable but are beyond the scope of this review.

3.2 Performing error evaluation from recent studies

~~SfM photogrammetry has been tested under a large variety of environments due to the commensurate novel establishment of the method in geosciences, revealing numerous advantages but also disadvantages regarding to each application. It is important to have method independent references to evaluate 3D reconstruction tools confidently. In total 39 studies are investigated (Table Appendix A), where a reference has been setup, either area~~

based (e.g. TLS) or point based (e.g. RTK-GPS points). Because not all studies perform accuracy assessment with independent references, the number of studies is in contrast to the number of 65 studies that are reviewed in regard to applications.

A designation of error parameters is performed prior to comparing the studies to avoid using ambiguous terms. There is a difference between local surface quality and more systematic errors, i.e. due to referencing and project geometry (James and Robson, 2012). Specifically, error can be assessed in regard to accuracy and precision.

Measurement accuracy, which defines the closeness of the measurement to a reference ideally displays the true surface and can be estimated by the mean error value. However, positive and negative deviations can compensate for each other and thus can impede the recognition of a systematic error (e.g. symmetric tilting) with the mean value. Therefore, numerical and spatial error distribution should also be considered to investigate the quality of the measurement (e.g. Smith et al., 2015). For the evaluation of two DEMs, the iterative closest point (ICP) algorithm can improve the accuracy significantly if a systematic linear error (e.g. shifts, tilts or scale variations) is given, as demonstrated by Micheletti et al. (2014). Nevertheless, this procedure can also induce an error when the scene has changed significantly between the two datasets.

Precision, which defines the repeatability of the measurement, e.g. it indicates how rough an actual planar surface is represented, usually comprises random errors that can be measured with the standard deviation or RMSE. However, precision is not independent from systematic errors. In this study, the focus lies on RMSE or standard deviation calculated to a given reference (e.g. to a LiDAR light detection and ranging point cloud) and thus the general term “measured error” is used.

Furthermore, error ratios are calculated to compare SfM photogrammetry performance between different studies under varying data acquisition and processing conditions. Thereby, the relative error (e_r), the reference superiority (e_s) and the theoretical error ratio (e_t) are considered. The first is defined as the ratio between measured error and surface to camera distance (eq. 1):

$$e_r = \frac{\sigma_m}{D} \quad (1)$$

Being:

e_r ...relative error

σ_m ...measured error

D ... mean distance camera — surface

The reference superiority displays the ratio between the measured error and the error of the reference (eq. 2). It depicts the validity of the reference to be accountable as a reliable dataset for comparison.

$$e_s = \frac{\sigma_m}{\sigma_{ref}} \quad (2)$$

Being:

e_s ... reference superiority

σ_{ref} ... reference error

The theoretical error ratio includes the theoretical error, which is an estimate of the theoretically best achievable photogrammetric performance under ideal conditions. It is calculated separately for convergent and parallel axes image acquisition schemes. The estimate of the theoretical error of depth measurement for the parallel-axis case is displayed by eq. 3 (more detail in Kraus, 2007). The error is determined for a stereo image pair and thus might overestimate the error for multi view reconstruction. Basically, the error is influenced by the focal length, the camera to surface distance and the distance between the images of the stereo pair (base).

$$\sigma_p = \frac{D^2}{Bc} \sigma_t \quad (3)$$

Being:

σ_p ... coordinate error for parallel axes case

c ... focal length

σ_t ... error image measurement

B ... distance between images (base)

For the convergent case the error also considers the camera to surface distance and the focal length. However, instead of the base the strength of image configuration determined by the angle between intersecting homologous rays is integrated and additionally the employed number of images is accounted for (eq. 4; more detail in Luhmann et al., 2014).

$$\sigma_e = \frac{qD}{\sqrt{k}c} \sigma_t \quad (4)$$

Being:

σ_e ... coordinate error for convergent case

q ... strength of image configuration, i.e. convergence

k ... number of images

Finally, the theoretical error ratio is calculated displaying the relation between the measured error and the theoretical error (eq. 5). The value depicts the performance of SfM photogrammetry in regard to the expected accuracy.

$$e_t = \frac{\sigma_m}{\sigma_{theo}} \quad (5)$$

Being:

e_t ... theoretical error ratio

σ_{theo} ... theoretical error; either σ_p or σ_e

The statistical analysis of the achieved precisions of the reviewed studies is performed with the Python Data Analysis Library (pandas). If several errors are given in one study due testing of different survey or processing conditions, the error value representing the enhancement of the SfM performance has been chosen, i.e. in the study of Javernick et al. (2014) the DEM without an error dome, of Rippin et al. (2015) the linear corrected DEM, and of Eltner & Schneider (2015) the DEMs calculated with undistorted images. In addition, if several approaches are conducted to retrieve the deviations value to the reference, the more reliable error measure is preferred (regards Stumpf et al., 2014 and Gómez Gutiérrez et al., 2014 and 2015). Apart from those considerations, measured errors have been averaged if several values are reported in one study, i.e. concerning multi temporal assessments or consideration of multiple surfaces with similar characteristics, but not for the case of different tested SfM tools. Regarding data visualisation, outliers that complicated plot drawing, were neglected within the concerning graphics. This concerned the study of Dietrich (2016) due to a very large scale of an investigated river reach (excluded from Fig. 4a and Fig. 5a-b), the study of Snapir et al. (2014) due to a very high reference accuracy of Lego bricks (excluded from Fig. 4e and Fig. 5b), and Frankl et al. (2015) due to a high measured error as the study focus was rather on feasibility than accuracy (excluded from Fig. 5c).

Besides exploiting a reference to estimate the performance of the 3D reconstruction, registration residuals of GCPs resulting from BA can be taken into account for a first error assessment. But it is not suitable as exclusive error measure due to potential deviations

~~between the true surface and the calculated statistical and geometric model, which are not detectable with the GCP error vectors alone because BA is optimised to minimise the error at these positions. However, if BA has been performed two staged (i.e. SfM and referencing calculated separately), the residual vector provides reliable quality information because registration points are not integrated into model estimation.~~

4—Recent applications of SfM photogrammetry in geosciences

The previously described advantages of the method has introduced a new group of users, leading to a variety of new studies in geomorphic surface reconstruction and analysis. Different disciplines started to use SfM algorithms more or less simultaneously.

A list of all topics reviewed in this manuscript according to their year of appearance is shown in Table 4. It is important to note that most subjects are not strictly separable from each other: For instance, a heavy flash flood event will likely trigger heavy damage by soil erosion or upstream slope failures. Thus, corresponding studies are arranged in regard to their major focus. The topic soil science comprises studies of soil erosion as well as soil micro-topography.

4.1 Soil science

An identification of convergent research topics of SfM photogrammetry in geosciences revealed a distinct focus on erosional processes, especially in soil erosion (11 studies). Gullies, as often unvegetated and morphologically complex features of soil erosion, are predestined to serve as a research object (6 studies) to evaluate SfM performance. One of the first works on SfM in geosciences from 2012 compared established 2D and 3D field methods for assessing gully erosion (e.g. LiDAR, profile meter, total station) to SfM data with regard to costs, accuracy and effectiveness revealing the superiority of the method (Castillo et al., 2012). Also for a gully system, Stöcker et al. (2015) demonstrated the flexibility of camera based surface reconstruction by combining independently captured terrestrial images with surface models from UAV images to fill data gaps and achieve a comprehensive 3D model. Large areal coverage and very high resolution - allowed for a new quality in the assessment of plot based soil erosion analysis (Eltner et al., 2015)

Another 6 studies tackle the 3D reconstruction of soil micro-topography by producing very dense point clouds or DEMs. This data further serves to assess pros and cons of SfM

Formatiert: Einzug: Links: 0 cm, Hängend: 0.75 cm, Mit Gliederung + Ebene: 2 + Nummerierungsformatvorlage: 1, 2, 3, ... + Beginnen bei: 1 + Ausrichtung: Links + Ausgerichtet an: 1.28 cm + Einzug bei: 1.91 cm

photogrammetry, e.g. to detect small-scale erosion features (Nouwakpo et al., 2014), with regard to the doming effect (Eltner and Schneider, 2015) or as input parameter for erosion modelling (Kaiser et al., 2015).

43.2 Volcanology

Volcanology is a pioneering area of SfM photogrammetry research in geosciences because 3 out of 6 studies in 2012 included volcanic research sites. James and Robson (2012) acquired information on volcanic dome volume and structural variability prior to an explosion from multi-temporal imagery taken from a light airplane. Another interesting work by Bretar et al. (2013) successfully reveals roughness differences in volcanic surfaces from lapilli deposits to slabby pahoehoe lava.

43.3 Glaciology

Glaciology and associated moraines are examined in 7 publications. In several UAV campaigns Immerzeel et al. (2014) detected limited mass losses and low surface velocities but high local variations of melt rates that are linked to supra-glacial ponds and ice cliffs. Rippin et al. (2015) present another UAV-based work on supra-glacial runoff networks, comparing the drainage system to surface roughness and surface reflectance measurements and detecting linkages between all three. Furthermore, snow depth estimation and rock glacier monitoring are increasingly performed with SfM photogrammetry (Nolan et al., 2015, Dall'Asta et al., 2015).

43.4 Mass movements

Compared to the well-established use of LiDAR techniques on the investigation of landslides (Jaboyedoff et al., 2012) the use of photogrammetric workflows for investigating hazardous slopes is still scarce, which is probably due to the stringent accuracy and safety requirements. For instance, the use of UAV systems for monitoring mass movements using both image correlation algorithms and DM subtraction techniques has been explored by Lucieer et al., (2013). More recently, SfM techniques were used by Stumpf et al. (2014) for monitoring landslide displacements and erosion during several measuring campaigns, including the study of seasonal dynamics on the landslide body, superficial deformation and

rock fall occurrence. In addition, these authors assessed the accuracy of two different 3D reconstruction tools compared to LiDAR data.

43.5 Fluvial morphology

Channel networks in floodplains were surveyed by Prosdocimi et al. (2015) in order to analyse eroded channel banks and to quantify the transported material. Besides classic DSLR cameras, evaluation of an iPhone camera revealed sufficient accuracy, so that in near future also non-scientist are able to carry out post event documentation of damage. An interesting large scale riverscape assessment is presented by Dietrich (2016), who carried out a helicopter based data acquisition of a 32 km river segment. A small helicopter proves to close the gap between unmanned platforms and commercial aerial photography from airplanes.

43.6 Coastal morphology

In the article by Westoby et al. (2012) several morphological features of contrasting landscapes were chosen to test the capabilities of SfM; one of them being a coastal cliff of roughly 80 m height. Up to 90.000 points/m² enabled the identification of bedrock faulting. Ružić et al. (2014) produced surface models of coastal cliffs to test the abilities of SfM photogrammetry in undercuts and complex morphologies.

43.7 Other fields of investigation in geosciences

In addition to the prevalent fields of attention also more exotic research is carried out unveiling unexpected possibilities for SfM photogrammetry. Besides the benefit for the specific research itself, these branches are important as they either explore new frontiers in geomorphometry or demonstrate the versatility of the method. Lucieer et al. (2014) analyse arctic moss beds and their health conditions by using high-resolution surface topography (2 cm DEM) to simulate water availability from snow melt. Leon et al. (2015) acquired underwater imagery of a coral reef to produce a DEM with a resolution of 1 mm for roughness estimation. Genchi et al. (2015) used UAV-image data of an urban cliff structure to identify bio erosion features and found a pattern in preferential locations.

The re-consideration of historical aerial images is another interesting opportunity arising from the new algorithmic image matching developments that allow for new DEM resolutions and thus possible new insights into landscape evolution (Gomez et al., 2015).

4 Error assessment of SfM photogrammetry in geo-scientific applications

SfM photogrammetry has been tested under a large variety of environments due to the commensurate novel establishment of the method in geosciences, revealing numerous advantages but also disadvantages regarding to each application. It is important to have method independent references to evaluate 3D reconstruction tools confidently. In total 39 studies are investigated (Table Appendix A), where a reference has been setup, either area based (e.g. TLS) or point based (e.g. RTK GPS points). Because not all studies perform accuracy assessment with independent references, the number of studies is in contrast to the number of 65 studies that are reviewed in regard to applications. In the following, methods are illustrated concerning integrated consideration of error performance of SfM photogrammetry in geo-scientific studies.

A designation of error parameters is performed prior to comparing the studies to avoid using ambiguous terms. There is a difference between local surface quality and more systematic errors, i.e. due to referencing and project geometry (James and Robson, 2012). Specifically, error can be assessed in regard to accuracy and precision.

Measurement accuracy, which defines the closeness of the measurement to a reference ideally displays the true surface and can be estimated by the mean error value. However, positive and negative deviations can compensate for each other and thus can impede the recognition of a systematic error (e.g. symmetric tilting) with the mean value. Therefore, numerical and spatial error distribution should also be considered to investigate the quality of the measurement (e.g. Smith et al., 2015). For the evaluation of two DEMs, the iterative closest point (ICP) algorithm can improve the accuracy significantly if a systematic linear error (e.g. shifts, tilts or scale variations) is given, as demonstrated by Micheletti et al. (2014); Nevertheless, this procedure can also induce an error when the scene has changed significantly between the two datasets.

Precision, which defines the repeatability of the measurement, e.g. it indicates how rough an actual planar surface is represented, usually comprises random errors that can be measured with the standard deviation or RMSE. However, precision is not independent from systematic errors. In this study, the focus lies on RMSE or standard deviation calculated to a given

reference (e.g. to a LiDAR - light detection and ranging - point cloud) and thus the general term “measured error” is used.

Furthermore, error ratios are calculated to compare SfM photogrammetry performance between different studies under varying data acquisition and processing conditions. Thereby, the relative error (e_r), the reference superiority (e_s) and the theoretical error ratio (e_t) are considered. The first is defined as the ratio between measured error and surface to camera distance (eq. 1).

$$e_r = \frac{\sigma_m}{D} \quad (1)$$

Being:

e_r ...relative error

σ_m ...measured error

D ...mean distance camera – surface

The reference superiority displays the ratio between the measured error and the error of the reference (eq. 2). It depicts the validity of the reference to be accountable as a reliable dataset for comparison.

$$e_s = \frac{\sigma_m}{\sigma_{ref}} \quad (2)$$

Being:

e_r ...reference superiority

σ_{ref} ...reference error

The theoretical error ratio includes the theoretical error, which is an estimate of the theoretically best achievable photogrammetric performance under ideal conditions. It is calculated separately for convergent and parallel-axes image acquisition schemes. The estimate of the theoretical error of depth measurement for the parallel-axis case is displayed by eq. 3 (more detail in Kraus, 2007). The error is determined for a stereo-image pair and thus might overestimate the error for multi-view reconstruction. Basically, the error is influenced by the focal length, the camera to surface distance and the distance between the images of the stereo-pair (base).

$$\sigma_p = \frac{D^2}{Bc} \sigma_i \quad (3)$$

Being:

σ_p ... coordinate error for parallel – axes case

c ... focal length

σ_i ... error image measurement

B ... distance between images (base)

For the convergent case the error also considers the camera to surface distance and the focal length. However, instead of the base the strength of image configuration determined by the angle between intersecting homologous rays is integrated and additionally the employed number of images is accounted for (eq. 4; more detail in Luhmann et al., 2014).

$$\sigma_c = \frac{qD}{\sqrt{k}c} \sigma_i \quad (4)$$

Being:

σ_c ... coordinate error for convergent case

q ... strength of image configuration, i.e. convergence

k ... number of images

Finally, the theoretical error ratio is calculated displaying the relation between the measured error and the theoretical error (eq. 5). The value depicts the performance of SfM photogrammetry in regard to the expected accuracy.

$$e_t = \frac{\sigma_m}{\sigma_{theo}} \quad (5)$$

Being:

e_t ... theoretical error ratio

σ_{theo} ... theoretical error; either σ_p or σ_c

The statistical analysis of the achieved precisions of the reviewed studies is performed with the Python Data Analysis Library (pandas). If several errors are given in one study due to testing of different survey or processing conditions, the error value representing the enhancement of the SfM performance has been chosen, i.e. in the study of Javernick et al. (2014) the DEM without an error dome, in the study of Rippin et al. (2015) the linear corrected DEM, and in the study of Eltner & Schneider (2015) the DEMs calculated with undistorted images. In addition, if several approaches are conducted to retrieve the deviations value to the reference, the more reliable error measure is preferred (regards Stumpf et al.,

2014 and Gómez-Gutiérrez et al., 2014 and 2015). Apart from those considerations, measured errors have been averaged if several values are reported in one study, i.e. concerning multi-temporal assessments or consideration of multiple surfaces with similar characteristics, but not for the case of different tested SfM tools. Regarding data visualisation, outliers that complicated plot drawing, were neglected within the concerning graphics. This concerned the study of Dietrich (2016) due to a very large scale of an investigated river reach (excluded from Fig. 4a and Fig. 5a-b), the study of Snapir et al. (2014) due to a very high reference accuracy of Lego bricks (excluded from Fig. 4c and Fig. 5b), and Frankl et al. (2015) due to a high measured error as the study focus was rather on feasibility than accuracy (excluded from Fig. 5c).

Besides exploiting a reference to estimate the performance of the 3D reconstruction, registration residuals of GCPs resulting from BA can be taken into account for a first error assessment. But it is not suitable as exclusive error measure due to potential deviations between the true surface and the calculated statistical and geometric model, which are not detectable with the GCP error vectors alone because BA is optimised to minimise the error at these positions. However, if BA has been performed two-staged (i.e. SfM and referencing calculated separately), the residual vector provides reliable quality information because registration points are not integrated into model estimation.

5—Error assessment of SfM photogrammetry in geo-scientific applications

Error evaluation in this study is performed with reference measurements. Thereby, errors due to the performance of the method itself and errors due to the method of quality assessment have to be distinguished.

5.1 Error sources of SfM photogrammetry

The error of 3D reconstruction is influenced by many factors: scale/distance, camera calibration, image network geometry, image matching performance, surface texture and lighting conditions, and GCP characteristics, which are examined in detail in this section.

4.1.1 Scale and sensor to surface distance

Formatiert: Schriftart: Nicht Kursiv

Formatiert: Überschrift 2, Abstand
Vor: 0 pt, Zeilenabstand: einfach

SfM photogrammetry contains the advantage to be useable at almost any scale. Thus, in the reviewed studies the method is applied at a large range of scales (Fig. 4a), reaching from 10 cm for volcanic bombs (Favalli et al., 2012, James and Robson, 2012) up to 10 km for a river reach (Dietrich, 2016). Median scale amounts about 100 m. SfM photogrammetry reveals a scale dependent practicability (Smith and Vericat, 2015) if case study specific tolerable errors are considered, e.g. for multi-temporal assessments. For instance, at plot and hillslope scale 3D reconstruction is a very sufficient method for soil erosion studies, even outperforming TLS (Nouwakpo et al., 2015, Eltner et al., 2015, Smith and Vericat, 2015). The method should be most useful in small scale study reaches (Fonstad et al., 2013), whereas error behaviour is not as advantageous for larger scales, i.e. catchments (Smith and Vericat, 2015).

Besides scale, the distance between sensor and surface is important for image-based reconstructed DEM error, also because scale and distance interrelate. The comparison of the reviewed studies indicates that with an increase of distance the measured error increases, which is not unexpected (Fig. 5a, circles). However, there is no linear trend detectable. Therefore, the relative error is not assignable. The relative error displays a large range from 15 to 4000 with a median of 400, thus revealing a rather low error potential (Fig. 5a, triangles). Very high ratios are solely observable for very close-range applications and at large distances. A general increase of the relative error with distance is observable (Fig. 5a, triangles). The indication that cm-accurate measurements are realisable at distances below 200 m (Stumpf et al., 2014) can be confirmed by Fig. 5a because most deviations are below 10 cm until that range. Overall, absolute error values are low at close ranges, whereas the relative error is higher at larger distances.

4.1.2 Camera calibration

SfM photogrammetry allows for straight forward handling of camera options due to integrated self-calibration, but knowledge about some basic parameters is necessary to avoid unwanted error propagation into the final DEM from insufficiently estimated camera models. The autofocus as well as automatic camera stabilisation options should be deactivated if a pre-calibrated camera model is used or one camera model is estimated for the entire image block because changes in the interior camera geometry due to camera movement cannot be captured with these settings. The estimation of a single camera model for one image block is usually preferable, if a single camera has been used, whose interior geometry is temporary stable, to

Formatiert: Schriftart: Nicht Kursiv

Formatiert: Überschrift 2, Abstand
Vor: 0 pt, Zeilenabstand: einfach

avoid over parameterisation (Pierrot-Deseilligny and Clery, 2011). Thus, if zoom lenses are moved a lot during data acquisition, they should be avoided due to their instable geometry (Shortis et al., 2006, Sanz-Ablanedo et al., 2010) that impedes usage of pre-calibrated fixed or single camera models. A good compromise between camera stability, sensor size and equipment weight, which is more relevant for UAV applications, are achieved by compact system cameras (Eltner and Schneider, 2015). However, solely three studies utilize compact system cameras in the reviewed studies (Tonkin et al., 2014, Eltner and Schneider, 2015, Eltner et al., 2015).

Along with camera settings, the complexity in regard to the considered parameters of the defined camera model within the 3D reconstruction tool is relevant as well as the implementation of GCPs to function as further observation in the BA, i.e. to avoid DEM domes as a consequence of insufficient image distortion estimation (James and Robson, 2014, Eltner and Schneider, 2015). Also, Stumpf et al. (2014) detect worse distortion correction with a basic SfM tool, considering a simple camera model, compared to more complex software, integrating a variety of camera models and GCP consideration. Camera calibration is a key element for high DEM quality, which is extensively considered in photogrammetric software, whereas simpler models that solely estimate principle distance and radial distortion are usually implemented in the SfM tools originating from computer vision (Eltner and Schneider, 2015, James and Robson, 2012, Pierrot-Deseilligny and Clery, 2011).

4.1.3 Image resolution

Image resolution is another factor influencing the final DEM quality. Especially, the absolute pixel size needs to be accounted for due to its relevance for the signal-to-noise ratio (SNR) because the larger the pixel the higher the amount of light that can be captured and hence a more distinct signal is measured. Resolution alone by means of pixel number gives no information about the actual metric sensor size. A large sensor with large pixels and a large amount of pixels provides better image quality due to reduced image noise than a small sensor with small pixels but the same amount of pixels. Thus, high image resolution defined by large pixel numbers and pixel sizes resolves in sufficient quality of images and thus DEMs (Micheletti et al., 2014, Eltner and Schneider, 2015).

However, the reviewed investigations indicate no obvious influence of the pixel size at the DEM quality. Mostly, cameras with middle sized sensors and corresponding pixel sizes around 5 μm are used and a large range of error at different pixel sizes is given.

Formatiert: Schriftart: Nicht Kursiv

Formatiert: Überschrift 2, Abstand
Vor: 0 pt, Zeilenabstand: einfach

To speed up processing, down-sampling of images is often performed causing interpolation of pixels and thus the reduction of image information, which can be the cause for underestimation of high relief changes, e.g., observed by Smith and Vericat (2015) or Nouwakpo et al. (2015). Interestingly, Prosdocimi et al. (2015) reveal that lower errors are possible with decreasing resolution due to an increase of error smoothing. Nevertheless, image data collection in the field should be done at highest realisable resolution and highest SNR to fully keep control over subsequent data processing, i.e. data smoothing should be performed under self-determined conditions at the desktop, which is especially important for studies of rough surfaces to allow for probate error statistics (e.g. Brasington et al., 2012).

4.1.4 Image network geometry

In regard to the geometry of the image network several parameters are important: number of images, image overlap, obliqueness and convergence.

At least three images need to capture the area of interest, but for redundancy to decrease DEM error higher numbers are preferred (James and Robson, 2012). For instance, Piermattei et al. (2015) detect better qualities for a higher amount of images. However, the increase of images does not linearly increase the accuracy (Micheletti et al., 2014), and may ultimately lead to unnecessary increase in computation time. Generally, image number should be chosen depending on the size and complexity of the study reach (James and Robson, 2012); as high as possible but still keeping in mind acceptable processing time.

High image overlap is relevant to finding homologous points within many images that cover the entire image space. Stumpf et al. (2014) show that higher overlap resolves in better results. Wide angle lenses, whose radial distortion is within the limits, should be chosen for data acquisition.

The reviewed studies reveal a large variety of applicable perspectives for DEM generation. Most applications use images captured from the ground, which is the most flexible implementation of the SfM photogrammetry method. In regard to terrestrial or aerial perspective, Smith and Vericat (2015) state that aerial images should be preferred if plots reach sizes larger 100 m because at these distances obliqueness of images becomes too adverse. Stumpf et al. (2014) even mention a distinct value of the incidence angle of 30° to the captured surface above which data quality decreases significantly.

Formatiert: Schriftart: Nicht Kursiv

Formatiert: Überschrift 2, Abstand
Vor: 0 pt, Zeilenabstand: einfach

Furthermore, image network geometry has to be considered separately for convergent acquisitions schemes, common for terrestrial data collection, and for parallel-axes acquisition schemes, common for aerial data collection. The parallel-axes image configuration results in unfavourable error propagation due to unfavourable parameter correlation, which inherits the separation between DEM shape and radial distortion (James and Robson, 2014, Wu, 2014) resulting in a dome error that needs either GCP implementation or a well estimated camera model for error mitigation (James and Robson, 2014, Eltner and Schneider, 2015). However, GCP accuracy has to be sufficient or else the weight of GCP information during BA is too low to avoid unfavourable correlations, as shown by Dietrich (2016), where DEM dome error within a river reach could not be diminished even though GCPs were implemented into 3D reconstruction. If convergent images are utilised, the angle of convergence is important because the higher the angle the better the image network geometry. Thereby, accuracy increases because sufficient image overlap is possible with larger bases between images. Therefore, glancing ray intersections, which impede distinct depth assignment, are avoided. But simultaneously, convergence should not be so high that the imaged scene becomes too contradictory for successful image matching (Pierrot-Deseilligny and Clery, 2012, Stöcker et al, 2015).

4.1.5 Accuracy and distribution of homologues image points

The quality of DEMs reconstructed from overlapping images depends significantly on the image-matching performance (Grün, 2012). Image content and type, which cannot be enhanced substantially, are the primary factors controlling the success of image-matching (Grün, 2012). Image-matching is important for reconstruction of the image network geometry as well as the subsequent dense-matching.

On the one hand, it is relevant to find good initial matches (e.g. SIFT features are not as precise as least square matches with $\frac{1}{10}$ pixel size accuracies; Grün, 2012) to perform reliable 3D reconstruction and thus retrieve an accurate sparse point cloud because optimization procedures for model refinement rely on this first point cloud. Thus, immanent errors will propagate along the different stages of SfM photogrammetry.

On the other hand, more obviously image-matching performance is important for dense reconstruction, when 3D information is calculated for almost every pixel. The accuracy of intersection during dense matching depends on the accuracy of the estimated camera orientations (Remondino et al., 2014). If the quality of the DEM is the primary focus, which is

Formatiert: Schriftart: Nicht Kursiv

Formatiert: Überschrift 2, Abstand
Vor: 0 pt, Zeilenabstand: einfach

usually not the case for SfM algorithms originating from computer vision, the task of image-matching is still difficult (Grün, 2012). Nevertheless, newer approaches are emerging, though, which still need evaluation in respect of accuracy and reliability (Remondino et al., 2014). An internal quality control for image-matching is important for DEM assessment (Grün, 2012), but are mostly absent in tools for SfM photogrammetry.

So far, many studies exist, which evaluate the quality of 3D reconstruction in geo-scientific applications. Nevertheless, considerations of dense-matching performance are still missing, especially in regard of rough topographies (Eltner and Schneider, 2015).

4.1.6 Surface texture

Texture and contrast of the area of interest is significant to identify suitable homologues image points. Low textured and contrasted surfaces result in a distinct decrease of image features, i.e. snow covered glaciers (Gómez-Gutiérrez et al., 2014) or sandy beaches (Mancini et al., 2013). Furthermore, vegetation cover complicates image matching performance due to its highly variable appearance from differing viewing angles (e.g. Castillo et al., 2012, Eltner et al., 2015) and possible movements during wind. Thus, in this study, where present, only studies of bare surfaces are reviewed for error assessment.

4.1.7 Illumination condition

Over- and under-exposure of images is another cause of error in the reconstructed point cloud, which cannot be significantly improved by utilising HDR images (Gómez-Gutiérrez et al., 2015). Well illuminated surfaces result in a high number of detected image features, which is demonstrated for coastal boulders under varying light conditions by Gienko and Terry (2014). Furthermore, Gómez-Gutiérrez et al. (2014) highlight the unfavourable influence of shadows because highest errors are measured in these regions; interestingly, these authors calculate the optimal time for image acquisition from the first DEM for multi-temporal data acquisition. Furthermore, the temporal length of image acquisition needs to be considered during sunny conditions because with increasing duration shadow changes can decrease matching performance, i.e. with regard to the intended quality surveys lasting more than 30 minutes should be avoided (Bemis et al., 2014). Generally, overcast but bright days are most suitable for image capture to avoid strong shadows or glared surfaces (James and Robson, 2012).

Formatiert: Schriftart: Nicht Kursiv

Formatiert: Überschrift 2, Abstand
Vor: 0 pt, Zeilenabstand: einfach

Formatiert: Schriftart: Nicht Kursiv

Formatiert: Überschrift 2, Abstand
Vor: 0 pt, Zeilenabstand: einfach

4.1.8 GCP accuracy and distribution

GCPs are important inputs for data referencing and scaling. Photogrammetry always stresses the weight of good ground control for accurate DEM calculation, especially if one-staged BA is performed. In the common SfM workflow integration of GCPs is less demanding because they are only needed to transform the 3D-model from the arbitrary coordinate system, which is comparable to the photogrammetric two-staged BA processing. A minimum of three GCPs are necessary to account for model rotation, translation and scale. However, GCP redundancy, thus more points, has been shown to be preferable to increase accuracy (James and Robson, 2012). A high number of GCPs further ensures the consideration of checkpoints not included for the referencing, which are used as independent quality measure of the final DEM. More complex 3D reconstruction tools either expand the original 3D-Helmert-transformation by secondary refinement of the estimated interior and exterior camera geometry to account for non-linear errors (e.g. Agisoft PhotoScan) or integrate the ground control into the BA (e.g. APERO). For instance, Javernick et al. (2014) could reduce the height error to decimetre level by including GCPs in the model refinement.

Natural features over stable areas, which are explicitly identifiable, are an alternative for GCP distributions, although they usually lack strong contrast (as opposed to artificial GCPs) that would allow for automatic identification and sub-pixel accurate measurement (e.g. Eltner et al., 2013). Nevertheless, they can be suitable for multi-temporal change detection applications, where installation of artificial GCPs might not be possible (e.g. glacier surface reconstruction; Piermattei et al., 2015) or necessary as in some cases relative accuracy is preferred over absolute performance (e.g. observation of landslide movements, Turner et al., 2015).

GCP distribution needs to be even and adapted to the terrain resulting in more GCPs in areas with large changes in relief (Harwin and Lucieer, 2012) to cover different terrain types. Harwin and Lucieer (2012) state an optimal GCP distance between $\frac{1}{5}$ and $\frac{1}{10}$ of object distance for UAV applications. Furthermore, the GCPs should be distributed widely across the target area (Smith et al., 2015) and at the edge or outside the study reach (James and Robson, 2012) to enclose the area of interest, because if the study area is extended outside the GCP area, a significant increase of error is observable in that region (Smith et al., 2014, Javernick et al., 2014, Rippin et al., 2015). If data acquisition is performed with parallel-axis UAV images and GCPs are implemented for model refinement, rules for GCP setup according to classical photogrammetry apply, i.e. dense GCP installation around the area of interest and height

Formatiert: Schriftart: Nicht Kursiv

Formatiert: Überschrift 2, Abstand
Vor: 0 pt, Zeilenabstand: einfach

851 control points in specific distances as function of image number (more detail in e.g. Kraus,
852 2007).

853 The measurement of GCPs can be performed either within the point cloud or the images,
854 preferring the latter because identification of distinct points in 3D point clouds of varying
855 density can be less reliable (James and Robson, 2012, Harwin and Lucieer, 2012) compared to
856 sub-pixel measurement in 2D images, where accuracy of GCP identification basically
857 depends on image quality. Fig. 5 a illustrates that only few studies measured GCPs in point
858 clouds producing higher errors compared to other applications at the same distance.

859

860 **54.2 Errors due to accuracy/precision assessment technique**

861 **4.2.1 Reference of superior accuracy**

862 It is difficult to find a suitable reference for error assessment of SfM photogrammetry in geo-
863 scientific or geomorphologic applications due to the usually complex and rough nature of the
864 studied surfaces. So far, either point based or area based measurements are carried out. On the
865 one hand, point based methods (e.g. RTK GPS or total station) ensure superior accuracy but
866 lack sufficient area coverage for precision statements of local deviations; on the other hand,
867 area based (e.g. TLS) estimations are used, which provide enough data density but can lack of
868 sufficient accuracy (Eltner and Schneider, 2015). Roughness is the least constrained error
869 within point clouds (Lague et al., 2013) independent from the observation method. Thus, it is
870 difficult to distinguish between method noises and actual signal of method differences,
871 especially at scales where the reference method reaches its performance limit. For instance
872 Tonkin et al. (2014) indicate that the quality of total station points is not necessarily superior
873 on steep terrain.

874 Generally, 75 % of the investigations reveal a measured error that is 20 times higher than the
875 error of the reference. But the median shows that the superiority of the reference accuracy is
876 actually significantly poorer; the measured error is merely twice the reference error (Fig. 4 c).
877 The reviewed studies further indicate that the superior accuracy of the reference seems to
878 depend on the camera-to-object distance (Fig. 5 b). In shorter distances (below 50 m) most
879 references reveal accuracies that are lower than one magnitude superiority to the measured
880 error. However, alternative reference methods are yet absent. Solely, for applications in
881 further distances the references are sufficient. These findings are relevant for the
882 interpretation of the relative error because low ratios at small scale reaches might be due to
883 the low performance of the reference rather than the actual 3D reconstruction quality but due

Formatiert: Schriftart: Nicht Kursiv

Formatiert: Überschrift 2, Abstand
Vor: 0 pt, Zeilenabstand: einfach

to the reference noise lower errors are not detectable. Low relative errors are measured where the superior accuracy is also low (distance 5-50 m) and large ratios are given at distance where superior accuracy increases as well.

4.2.2 Type of deviation measurement

The reviewed studies use different approaches to measure the distance between the reference and the 3D reconstructed surface. Comparisons are either performed in 2.5D (raster) or real 3D (point cloud). Lague et al. (2013) highlight that the application of raster inherits the disadvantage of data interpolation, especially relevant for rough surfaces or complex areas (e.g. undercuts as demonstrated for gullies by Frankl et al., 2015). In this context it is important to note that lower errors are measured for point-to-point distances rather than raster differencing (Smith and Vericat, 2015, Gómez-Gutiérrez et al., 2014b).

Furthermore, within 3D evaluation different methods for deviation measurement exist. The point-to-point comparison is solely suitable for a preliminary error assessment because this method is prone to outliers and differing point densities. By point cloud interpolation alone (point-to-mesh), this issue is not solvable because there are still problems at very rough surfaces (Lague et al., 2013). Different solutions have been proposed: On the one hand, Abellan et al. (2009) proposed averaging the point cloud difference along the spatial dimension, which can also be extended to 4D (x, y, z, time; Kromer et al., 2015). On the other hand, Lague et al. (2013) proposed the M3C2 algorithm for point cloud comparison that considers the local roughness and further computes the statistical significance of detected changes. Stumpf et al. (2014) and Gómez-Gutiérrez et al. (2015) illustrated lower error measurements with M3C2 compared to point-to-point or point-to-mesh. Furthermore, Kromer et al. (2015) showed how the 4D filtering, when its implementation is feasible, allows to considerably increase the level of detection compared to other well-established techniques of comparison.

54.3 Standardised error assessment

To compare the achieved accuracies and precisions of different studies a standardised error assessment is necessary, e.g. considering the theoretical error ratio. The calculation of the theoretical error for the convergent image acquisition schemes is possible, making some basic assumptions about the network geometry, i.e. the strength of image configuration equals 1 (as in James & Robson, 2012), the number of images equals 3 (as in James & Robson, 2012) and

Formatiert: Schriftart: Nicht Kursiv

Formatiert: Überschrift 2, Abstand
Vor: 0 pt, Zeilenabstand: einfach

an image measurement error of 0.29 due to quantisation noise (as a result of continuous signal conversion to discrete pixel value). However, it is not possible to evaluate the theoretical error for parallel-axes case studies because information about the distance between subsequent images (base) is mostly missing, but essential to solve the equation and should not be assumed. Eltner and Schneider (2015) and Eltner et al. (2015) compare their results to parallel-axes theoretical error and could demonstrate that for soil surface measurement from low flying heights at least photogrammetric accuracy is possible (e.g. sub-cm error for altitudes around 10 m).

The results from James and Robson (2012), which show a less reliable performance of SfM than expected from photogrammetric estimation, can be confirmed by the reviewed studies. Image-based 3D reconstruction, considering SfM workflows, performs poorer than the theoretical error (Fig. 5c). The measured error is always higher and on average 90 times worse than the theoretical error. Even for the smallest theoretical error ratio the actual error is 6 times higher. Furthermore, it seems that with increasing distance theoretical and measured errors converge slightly.

As demonstrated, diverse factors influence SfM photogrammetry performance and subsequent DEM error with different sensitivity. Generally, accurate and extensive data acquisition is necessary to minimise error significantly (Javernick et al., 2014). Independent reference sources, such as TLS, are not replaceable (James and Robson, 2012) due to their differing error properties (i.e. error reliability) compared to image-matching (Grün, 2012). Synergetic effects of SfM and classical photogrammetry should be used, i.e. benefiting from the high automation of SfM to retrieve initial estimates without any prior knowledge about the image scene and acquisition configuration and adjacent reducing error by approved photogrammetric approaches, which are optimised for high accuracies.

The reviewed studies indicate the necessity of a standardised protocol for error assessment because the variety of studies inherit a variety of scales worked at, software used, GCP types measured, deviation measures applied, image network configurations implemented, cameras and platforms operated and reference utilised, making it very difficult to compare results with consistency. Relevant parameters for a standard protocol are suggested in Table 5.

65 Perspectives and limitations

SfM photogrammetry has allowed capturing massive three-dimensional datasets by non-specialists during the last five years, and it is highly expected that this technique will evolve

during the forthcoming decade. Current studies are focusing on capturing the terrain's geometry with high precision, but several opportunities to improve our understanding, modelling and prediction of different earth surface processes still remain unexplored. For instance, the use of super-macro imagery in conventional SfM workflows is expected to be explored soon for investigating natural phenomena in a much higher level of detail. Nevertheless, some technological issues that need to be addressed include the progressive degradation of the data quality at very short distances due to the effect of a limited depth of field; Up to our knowledge, the use of focus stacking for extending shallow depth of field of single images has not been explored yet. Some other technical and operational aspects are still limiting our ability to derive 3D point clouds from digital imagery over naturally complex outcrops. Examples include the occurrence of biases and occlusions that can strongly influence the quality of the acquired datasets and the progressive reduction of the ground resolution (meter/pixel) at longer distances, which can be addressed using mobile platforms such as UAV systems. Eventually, SfM photogrammetry technique may become a mainstream procedure in geomorphological studies during the next decade, perspectives include efforts in cross-disciplinarity, process automatisation, data and code sharing, real time data acquisition and processing, unlocking the archives, etc., as follows:

6.5.1 Cross-disciplinarity

A great potential relies on adapting three dimensional methods originally developed for the treatment of 3D LiDAR data to investigate natural phenomena through SfM photogrammetry techniques. Applications on 3D point cloud treatment dating back from the last decade will soon be integrated into SfM photogrammetry post-processing; Examples include: geomorphological investigations in high mountain areas (Milan et al., 2007), geological mapping (Buckley et al., 2008; Franceschi et al. 2009), soil erosion studies (Eltner and Baumgart, 2015), investigation of fluvial systems (Heritage and Hetherington, 2007, Cavalli et al., 2008; Brasington et al., 2012), and mass wasting phenomena (Lim et al., 2005, Oppikofer et al. 2009, Abellan et al., 2010).

Some other data treatment techniques that have been developed during the last decade and that will be adapted and enriched by the growing SfM photogrammetry community include: automatic lithological segmentation according to the intensity signature (Humair et al., 2015), integration of ground based LiDAR with thermal/hyperspectral imaging for lithological discrimination (Kääb, 2008, Hartzell et al., 2014), extraction of the structural settings on a

given outcrop (Jaboyedoff et al., 2007, Sturzenegger and Stead, 2009, Gigli and Casagli, 2011, Riquelme et al., 2014) and the automatic extraction of geological patterns such as surface roughness (Poropat, 2009), discontinuity spacing/persistence/waviness (Fekete et al. 2010, Khoshelham et al., 2011, Pollyea and Fairley, 2011). Concerning 4D data treatment for investigating changes on natural slope, some lessons learned may be adapted from the bi- and three-dimensional tracking of mass movements (Teza et al., 2007, Monserrat and Crosetto 2008), investigation of progressive failures (Royan et al., 2015, Kromer et al., 2015), and from the usage of mobile systems (Lato et al., 2009, Michoud et al., 2015).

6.2 Process-automatisation

~~Handling huge databases is an important issue and although fully automatic techniques may not be necessary in some applications, a series of tedious and manual processes are still required for data treatment.~~

6.3.2 Data and code sharing

Open data in geomorphometric studies using point clouds is also needed. The development of open-source software for handling huge 3D datasets such as CloudCompare (Girardeau-Montaut, 2015) has considerably boosted geomorphometric studies using 3D point clouds due to providing facile processing of such memory intense data. Nevertheless, apart from the above mentioned case, sharing the source code or the RAW data of specific applications for investigating earth surface processes is still not well established in our discipline. A series of freely available databases exist for LiDAR datasets (openTopography.org, rockbench.com, 3D-landslide.com). But up to the knowledge of these authors, there is no specific Git-Hub cluster or website dedicated to the maintaining and development of open-access software in geosciences.

6.4.3 Unlocking the archive

The appraisal of digital photography and the exponential increase of data storage capabilities have enabled the massive archive of optical images around the world. Accessing such quantity of information could provide unexpected opportunities for the four dimensional research of geomorphological processes using SfM photogrammetry workflows. Except for some open repositories (e.g. Flickr, Google ~~s~~Street ~~*V~~iew) the possibility to access the

1015 massive optical data is still scarce. In addition, accessing to such databases may become a
1016 challenging task due to data interchangeability issues. A considerable effort may be necessary
1017 for creating such database with homogeneous data formats and descriptors (type of
1018 phenomenon, temporal resolution, pixel size, accuracy, distance to object, existence of GCPs,
1019 etc.) during the forthcoming years.

1020 A first valuable approach to use data from online imagery was presented by Martin-Brualla et
1021 al. (2015), who pave the way for further research in a new field of 3D surface analysis (i.e.
1022 time-lapse). Other possible applications might unlock the archive of ancient airborne,
1023 helicopter-based or terrestrial imagery, ranging from the estimation of coastal retreat rates,
1024 the observation of the evolution of natural hazards to the monitoring of glacier fronts, and
1025 further.

1026

1027 **65.5-4 Real time data acquisition**

1028 Rapid developments in automatisisation (soft- and hardware wise) allow for in situ data
1029 acquisition and its immediate transfer to processing and analysing institutions. Thus, extreme
1030 events are recognisable during their occurrence and authorities or rescue teams can be
1031 informed in real-time. In this context SfM photogrammetry could help to detect and quantify
1032 rapid volume changes of e.g. glacier fronts, pro-glacial lakes, rock failures and ephemeral
1033 rivers.

1034 Furthermore, real-time crowd sourcing offers an entirely new dimension of data acquisition.
1035 Due to the high connectivity of the public through smartphones, various possibilities arise to
1036 share data (Johnson-Roberson et al., 2015). An already implemented example is real-time
1037 traffic information. Jackson and Magro (2015) name further options. Crowd sourced imagery
1038 can largely expand possibilities to 3D information.

1039

1040 **65.6-5 Time-lapse photography**

1041 A limited frequency of data acquisition increases the likelihood of superimposition and
1042 coalescence of geomorphological processes (Abellan et al., 2014). Since time-lapse SfM
1043 photogrammetry data acquisition has remained so far unexplored, a great prospect is expected
1044 on this topic during the coming years. To date solely James and Robson (2014b) demonstrated
1045 its potential by monitoring a lava flow at minute intervals for 37 minutes. One reason why

1046 time-lapse SfM photogrammetry remains rather untouched in geosciences lies in the complex
1047 nature of producing continuous data sets.

1048 Besides the need for an adequate research site (frequent morphodynamic activity), other
1049 aspects have to be taken into account: an automatic camera setup is required with self-
1050 contained energy supply (either via insolation or wind), adequate storage and appropriate
1051 choice of viewing angles onto the area of interest. Furthermore, cameras need to comprise
1052 sufficient image overlap and have to be synchronised. Ground control is required and an
1053 automatic pipeline for large data treatment should be developed.

1054 New algorithms are necessary to deal with massive point cloud databases. Thus, innovative
1055 four dimensional approaches have to be developed to take advantage of the information
1056 contained in real-time and/or time-lapse monitoring. Furthermore, Handling huge databases
1057 is an important issue and although fully automatic techniques may not be necessary in some
1058 applications, a series of tedious and manual processes are still required for data treatment.

1059 Combining real-time and/or time-lapse ~~these~~ datasets with climatic information can improve
1060 the modelling of geomorphological processes.

1061

1062 **65.7-6 Automatic UAV surveying**

1063 Unmanned airborne vehicles already show a large degree of automatisisation as they follow
1064 flight paths and acquire data autonomously. Human control is not required except for
1065 launching of the multi-copter or fixed wing system. Automatic landing is already provided by
1066 several systems. In near future a fully automatic UAV installation could comprise the
1067 following: repeated survey of an area of interest, landing and charging at a base station, data
1068 link for local storage or satellite based data transfer, and safety mechanism for preventing lift-
1069 off during inappropriate weather conditions. However, a large limitation for such realisation
1070 lies in legal restrictions because national authorities commonly request for visual contact to
1071 the UAV in case of failure. But in remote areas installation of an automatic system could
1072 already be allowed by regulation authorities.

1073

1074 **65.8-7 Direct geo-referencing**

1075 The use of GCPs is very time-consuming in the current SfM workflow. At first, field efforts
1076 are high to install and measure the GCPs during data acquisition. Afterwards, again much

time and labour is required during post-processing in order to identify the GCPs in the images, although some progress is made regarding to automatic GCP identification, e.g. by the exploitation of templates (Chen et al., 2000). The efficiency of geo-referencing can be increased significantly applying direct geo-referencing. Thus, the location and position of the camera is measured in real time and synchronised to the image capture by an on-board GPS receiver and IMU (inertial measurement unit) recording camera tilts. This applies to UAV systems as well as terrestrial data acquisition, e.g. by smartphones (Masiero et al., 2014). Exploiting direct geo-referencing can reduce usage of GCPs to a minimum or even replace it, which is already demonstrated by Nolan et al. (2015), who generated DEMs with spatial extents of up to 40 km² and a geo-location accuracy of ± 30 cm.

The technique can be very advantageous when it comes to monitoring areas with great spatial extents or inaccessible research sites. However, further development is necessary, thereby focusing on light-weighted but precise GPS receivers and IMU systems; on UAVs due to their limited payload and for hand-held devices due to their feasibility (e.g. Eling et al., 2015).

1091

1092

1093 **76 Conclusions**

This review has shown the versatility and flexibility of the recently established method SfM photogrammetry. Due to its beneficial qualities, a wide community of geoscientists starts to implement 3D reconstruction based on images within a variety of studies. Summing up the publications, there are no considerable disadvantages mentioned (e.g. accuracy wise) compared to other methods that cannot be counteracted by placement of GCPs, camera calibration or a high image number. Frontiers in geomorphometry have been expanded once more, as limits of other surveying techniques such as restricted mobility, isolated area of application and high costs are overcome by the SfM photogrammetry. Its major advantages lie in easy-to-handle and cost-efficient digital cameras as well as non-commercial software solutions.

SfM photogrammetry is already becoming an essential tool for digital surface mapping. It is employable in a fully automatic manner but individual adjustments can be conducted to account for each specific case study constrain and accuracy requirement in regard to the intended application. Due to the possibility of different degrees of process interaction, non-experts can utilise the method depending on their discretion.

1109 While research of the last years mainly focussed on testing the applicability of SfM
1110 photogrammetry in various geo-scientific applications, recent studies try to pave the way for
1111 future usages and develop new tools, setups or algorithms. Performance analysis revealed the
1112 suitability of SfM photogrammetry at a large range of scales in regard to case study specific
1113 accuracy necessities. However, different factors influencing final DEM quality still need to be
1114 addressed. This should be performed under strict experimental (laboratory) designs because
1115 complex morphologies, typical in earth surface observations, impede accuracy assessment due
1116 to missing superior reference. Thus, independent references and GCPs are still needed in SfM
1117 photogrammetry for reliable estimation of the quality of each 3D reconstructed surface.

1118
1119 Fast and straightforward generation of DEMs using freely available tools produces new
1120 challenges. The exploitation of the entire information of the SfM photogrammetry output (3D
1121 point cloud or mesh instead of 2.5D raster) will become a significant challenge in future
1122 studies of high resolution topography (Passalacqua et al., 2015), which has to be even
1123 extended to 4D when investigating the evolution along time. Thus, especially comprehensive
1124 end user software needs further progress in these aspects.

1125

1126 **Appendix A:**

1127 Summary of information about reviewed studies used for application evaluation and performance assessment of SfM photogrammetry. Variables are
1128 explained in chapter 5.

ID	Author	Year	Application	Software	Perspective	Distance [m]	Scale* [m]	Pixel size [μm]	Image number	Complexity of SfM tool	Measurement error [mm]	Relative error	reference superiority	Theoretical error ratio
1	Castillo et al.	2012	gully erosion	Bundler + PMVS2	terrestrial	7	7	5.2	191	basic	20	350	-	79
2	Castillo et al.	2014	ephemeral gully erosion	Bundler + PMVS2	terrestrial	6	25	5.2	515	basic	22	273	11	101
3	Castillo et al.	2015	gully erosion	SF3M	terrestrial	10	350	1.5	3095	basic	69	145	3.45	455
4	Dietrich	2016	riverscape mapping	PhotoScan	helicopter	200	10000	4.3	1483	complex	730	274	-	-
5	Eltner et al.	2015	soil erosion	Pix4D	UAV	10	30	2.0, 5.0	100	complex	5, 6	2000, 1667	-	-
6	Eltner and Schneider	2015	soil roughness	VisualSfM + PMVS2, PhotoScan, Pix4D, APERO + MicMac, Bundler + PMVS2	UAV	12	15	5.0	13	basic, complex	8.1 - 9.8	1224 - 1481	-	-
7	Favalli et al.	2012	geological outcrops, volcanic bomb, stalagmite	Bundler + PMVS2	terrestrial	1	0.1 - 0.3	5.2	30 - 67	basic	0.3 - 3.8	367 - 3333	-	-
8	Fonstad et al.	2013	bedrock channel and floodplain	Photosynth (Bundler implementation)	terrestrial	40	200	1.7	304	basic	250	160	2	139
9	Frankl et al.	2015	gully	PhotoScan	terrestrial	2	10	5.2	180 -	complex	17 - 190	11 - 147	0 - 4	156 - 2184

			measurement					235						
10	Genchi et al.	2015	bioerosion pattern	VisualSfM + PMVS2	UAV	20	100	1.5	400	basic	35	571	-	29
11	Gómez-Gutiérrez et al.	2014	gully headcut	123D Catch	terrestrial	9.3 - 10.5	10	4.3	41 - 93	basic	12 - 32	291 - 792	-	31 - 85
12	Gómez-Gutiérrez et al.	2014	rock glacier	123D Catch	terrestrial	300	130	8.2	6	basic	430	698	72	103
13	Gómez-Gutiérrez et al.	2015	rock glacier	123D catch, PhotoScan	terrestrial	300	130	8.2	9	basic, complex	84 - 1029	-	-	-
14	Immerzeel et al.	2014	dynamic of debris covered glacial tongue	PhotoScan	UAV	300	3500	1.3	284, 307	complex	330	909	-	-
15	James and Robson	2012	volcanic bomb, summit crater, coastal cliff	Bundler + PMVS2	terrestrial, UAV	0.7 - 1000	0.1 - 1600	5.2, 7.4	133 - 210	basic	1000 - 2333	0 - 62	1 - 12	16 - 25
16	Javernick et al.	2014	braided river	PhotoScan	helicopter	700	1500	-	147	complex	170	4118	3	-
17	Johnson et al.	2014	alluvial fan, earthquake scarp	PhotoScan	UAV	50, 60	300, 1000	4.8	233, 450	complex	130 - 410	122 - 385	-	-
18	Kaiser et al.	2014	gully and rill erosion	PhotoScan	terrestrial	5	10	6.4	-	complex	73 - 141	35 - 68	-	232 - 447
19	Leon et al.	2015	coral reef roughness	PhotoScan	terrestrial (marine)	1.5	250	1.5	1370	complex	0.6	2500	-	-
20	Mancini et al.	2013	fore dune	PhotoScan	UAV	40	200	4.3	550	complex	110 - 190	211 - 364	4	-
21	Micheletti et al.	2014	river bank, alluvial fan	123D Catch	terrestrial	10, 345	10, 300	4.8, 1.8	13	complex	16.8 - 526.3	327 - 595	-	40 - 73
22	Nadal-Romero et al.	2015	badland erosion	PhotoScan	terrestrial	50, 125	50, 100	5.5	15, 17	complex	14 - 33	2500 - 4032	1 - 2	6 - 10

23	Nouwakpo et al.	2015	microtopography erosion plots	PhotoScan	terrestrial	2	6	6.4	25	complex	5	400	-	-
24	Ouédraogo et al.	2014	agricultural watershed	Apero + MicMac, PhotoScan	UAV	100	200	2.0	760	complex	90, 139	1111, 719	-	6, 9
25	Piermattei et al.	2015	debris covered glacier monitoring	PhotoScan	terrestrial	100	350	4.8, 6.3	35, 47	complex	300, 130	333, 769	2, 1	56, 35
26	Prosdocimi et al.	2015	channel bank erosion	PhotoScan	terrestrial	7	30	1.4 - 6.3	60	complex	57 - 78	90 - 123	1	143 - 373
27	Rippin et al.	2015	supra-glacial hydrology	PhotoScan	UAV	121	2000	2.2	423	complex	400	303	-	-
28	Ruzic et al.	2014	coastal cliff	Autodesk ReCap	terrestrial	15	50	2.0	250	basic	70	214	1	82
29	Smith et al.	2014	post-flash flood evaluation	PhotoScan	terrestrial	50	150	1.7	-	complex	135	370	14	39
30	Smith and Vericat	2015	badland changes at different scales	PhotoScan	terrestrial, UAV, AutoGiro	5 - 250	20 - 1000	1.7, 5.5	30 - 527	complex	12.8 - 445	132 - 974	2 - 89	36 - 107
31	Snafir et al.	2014	roughness of soil surface	SfMToolkit	terrestrial	0.6	3	4.3	700	basic	2.7	222	270	-
32	Stumpf et al.	2014	landslide scarp	VisualSfM + CMVS, APERO + MicMac	terrestrial	50	750	8.5	88 - 401	basic, complex	27 - 232	667 - 1852	1 - 3	13 - 64
33	Tamminga et al.	2015	change detection after extreme flood event	EnsoMOSAIC UAV	UAV	100	200	1.3	310	complex	47	2128	2	-
34	Tonkin et al.	2014	moraine-mound topography	PhotoScan	UAV	100	500	4.3	543	complex	517	193	-	-
35	Turner et al.	2015	landslide change detection	PhotoScan	UAV	40	125	4.3	62 - 415	complex	31 - 90	444 - 1290	1 - 3	-
36	Westoby et al.	2012	coastal cliff	SfMToolkit	terrestrial	15	300	4.3	889	basic	500	100	-	-
37	Westoby et	2014	moraine dam,	SfMToolkit3	terrestrial	500	500	4.3	1002,	basic	814, 85	614,	2, 43	-

al.			alluvial debris fan					1054				1176		
38	Woodget et al.	2015	fluvial topography	PhotoScan	UAV	26 - 28	50, 100	2.0	32 - 64	complex	19 - 203	138 - 1421	-	-
39	Zarco-Tejada et al.	2014	tree height estimation	Pix4D	UAV	200	1000	4.3	1409	complex	350	571	23	-
40	Bemis et al.	2014	structural geology	PhotoScan	UAV, terrestrial	-	-	-	-	-	-	-	-	-
41	Bendig et al.	2013	crop growth	PhotoScan	UAV	30	7	-	-	-	-	-	-	-
42	Bini et al.	2014	coast erosion/abrasion	Bundler	terrestrial	-	-	-	-	-	-	-	-	-
43	Bretar et al.	2013	(volcanic) surface roughness	APER0 + MicMac	terrestrial	1.5	5.9 - 24.6	-	-	-	-	-	-	-
44	Brothelande et al.	2015	post-caldera resurgence	PhotoScan	aircraft	150	6000	8.2	7000	-	3100	48	62	-
45	Burns et al.	2015	coral reef	Photoscan	terrestrial (marine)	2	28	-	-	-	-	-	-	-
46	Clapuyt et al.	2015	slope morphology	VisualSFM	UAV	50	100	-	-	-	-	-	-	-
47	Dall'Asta et al.	2015	rock glacier monitoring	APER0 + MicMac, Photoscan	UAV	150		-	-	-	-	-	-	-
48	Dandois and Ellis	2013	vegetation mapping	Photoscan	UAV	130	250	-	-	-	-	-	-	-
49	Fernández et al.	2015	landslide	Photoscan	UAV	90	250	-	-	-	-	-	-	-
50	Gienko and Terry	2014	coastal boulders	Photoscan	terrestrial	3	2.5	-	-	-	-	-	-	-
51	Fugazza et al.	2015	glacier mapping	Menci APS	UAV	250	500	-	-	-	-	-	-	-
52	Gomez	2014	volcano morphology	Photoscan	aircraft	-	10000	-	-	-	-	-	-	-
53	Harwin and Lucieer	2012	coastal erosion	Bundler + PMVS2	UAV	120	100	-	1	-	-	-	-	-

54	James and Varley	2012	volcanic dome control	Bundler Photogrammetry package	aircraft	505 – 2420	250	-	-	-	-	-	-	-
55	Kaiser et al.	2015	soil hydraulic roughness	PhotoScan	terrestrial	0.5	1	-	-	-	-	-	-	-
56	Lucieer et al.	2013	landslide	PhotoScan	UAV	40	125	-	-	-	-	-	-	-
57	Lucieer et al.	2014	antartic moss beds	PhotoScan	UAV	50	64	-	-	-	-	-	-	-
58	Meesuk et al.	2014	Urban flooding	VisualSfM	terrestrial	-	-	-	-	-	-	-	-	-
59	Morgenroth and Gomez	2014	tree structure	Photoscan	terrestrial	5	5	-	-	-	-	-	-	-
60	Nouwakpo et al.	2014	soil microtopography	Photoscan	terrestrial	3.1	10	-	-	-	-	-	-	-
61	Stöcker et al.	2015	gully erosion	APERIO + MicMac	terrestrial + UAV	2 + 15	35	-	-	-	-	-	-	-
62	Ryan et al.	2015	glacier drainage observation	Photoscan	UAV	500	5000	-	-	-	-	-	-	-
63	Torres-Sánchez et al.	2015	tree plantation	Photoscan	UAV	50, 100	-	-	-	-	-	-	-	-
64	Turner et al.	2015	landslide monitoring	Bundler + PMVS2	UAV	50	-	-	-	-	-	-	-	-
65	Vasuki et al.	2014	structural geology	Bundler + PMVS2	UAV	30 - 40	100	-	-	-	-	-	-	-

1129

1130 **These studies are considered for performance analysis.**

1131 *For most authors not all camera parameters are given. Hence, camera parameters are retrieved from dpreview.com (or similar sources).*

1132 * If scale or distance is not given, they are estimated from study area display.

1133 **Acknowledgements**

1134 The authors A. Eltner, A. Kaiser and F. Neugirg are funded by the German Research
1135 Foundation (DFG) (MA 2504/15-1, HA5740/3-1, SCHM1373/8-1). A. Abellan acknowledges
1136 support by the Risk Analysis group (Univ. Lausanne) and the UPC (RockRisk research
1137 project BIA2013-42582-P).

1138 We would like to thank an anonymous referee and Matt Westoby for their remarks, which
1139 significantly improved the manuscript.

1140

1141 **References**

1142 Abellán, A., Jaboyedoff, M., Oppikofer, T. and Vilaplana, J. M.: Detection of millimetric
1143 deformation using a terrestrial laser scanner: experiment and application to a rockfall event,
1144 Nat. Hazard Earth Sys., 9, 365–372, 2009.

1145 Abellán, A., Calvet, J., Vilaplana, J. M. and Blanchard, J.: Detection and spatial prediction of
1146 rockfalls by means of terrestrial laser scanner monitoring, Geomorphology, 119, 162–171,
1147 doi:10.1016/j.geomorph.2010.03.016, 2010.

1148 Abellán, A., Oppikofer, T., Jaboyedoff, M., Rosser, N. J., Lim, M. and Lato, M. J.: Terrestrial
1149 laser scanning of rock slope instabilities, Earth Surf. Proc. Landf., 39(1), 80–97.
1150 doi:10.1002/esp.3493, 2014.

1151 Ai, M., Hu, Q., Li, J., Wang, M., Yuan, H. and Wang, S.: A Robust Photogrammetric
1152 Processing Method of Low-Altitude UAV Images, Remote Sensing, 7, 2302–2333,
1153 doi:10.3390/rs70302302, 2015.

1154 Astre, H.: SfMtoolkit. <http://www.visual-experiments.com/demos/sfmtoolkit/>, last access
1155 Nov. 2015.

1156 Bemis, S. P., Micklethwaite, S., Turner, D., James, M. R., Akciz, S., Thiele, S. T. and
1157 Bangash, H. A.: Ground-based and UAV-Based photogrammetry: A multi-scale, high-
1158 resolution mapping tool for structural geology and paleoseismology, J. Struct. Geol., 69, 163–
1159 178, doi:10.1016/j.jsg.2014.10.007, 2014.

1160 Bendig, J., Bolten, A. and Bareth, G.: UAV-based Imaging for Multi-Temporal, very high
1161 Resolution Crop Surface Models to monitor Crop Growth Variability, Photogramm.
1162 Fernerkun., 6, 551–562, doi:10.1127/1432-8364/2013/02001, 2013.

1163 Bini, M., Isola, I., Pappalardo, M., Ribolini, A., Favalli, M., Ragaini, L. and Zanchetta, G.:
 1164 Abrasive notches along the Atlantic Patagonian coast and their potential use as sea level
 1165 markers: the case of Puerto Deseado (Santa Cruz, Argentina), *Earth Surf. Proc. Landf.*, 39,
 1166 1550–1558, doi:10.1002/esp.3612, 2014.

1167 Bracken, L. J., Turnbull, L., Wainwright, J. and Bogaart, P.: State of Science Sediment
 1168 connectivity: a framework for understanding sediment transfer at multiple scales, *Earth Surf.*
 1169 *Proc. Landf.*, 40, 177–188, doi:10.1002/esp.3635, 2015.

1170 Brasington, J., Vericat, D. and Rychkov, I.: Modeling river bed morphology, roughness, and
 1171 surface sedimentology using high resolution terrestrial laser scanning, *Water Resources*
 1172 *Research*, 48, W11519, doi:10.1029/2012WR012223, 2012.

1173 Bretar, F., Arab-Sedze, M., Champion, J., Pierrot-Deseilligny, M., Heggy, E. and
 1174 Jacquemoud, S.: An advanced photogrammetric method to measure surface roughness:
 1175 Application to volcanic terrains in the Piton de la Fournaise, Reunion Island, *Remote Sens.*
 1176 *Environ.*, 135, 1–11, doi:10.1016/j.rse.2013.03.026, 2013.

1177 Brothelande, E., Lénat, J.-F., Normier, A., Bacri, C., Peltier, A., Paris, R., Kelfoun, K., Merle,
 1178 O., Finizola, A. And Garaebiti, E.: Insights into the evolution of the Yenkahe resurgent dome
 1179 (Siwi caldera, Tanna Island, Vanuatu) inferred from aerial high-resolution photogrammetry, *J.*
 1180 *Volcanol. Geoth. Res.*, doi:10.1016/j.jvolgeores.2015.04.006, 2015.

1181 Brown, M. Z., Burschka, D. and Hager, G. D.: Advances in Computational Stereo, in: *IEEE*
 1182 *Transactions on pattern analysis and machine intelligence*, 25, 993–1008, 2003.

1183 Buckley, S., Howell, J., Enge, H. and Kurz, T.: Terrestrial laser scanning in geology: data
 1184 acquisition, processing and accuracy considerations, *J. Geol. Soc. London*, 165, 625–638,
 1185 2008.

1186 Burns, J. H. R., Delparte, D., Gates, R. D. and Takabayashi, M.: Integrating structure-from-
 1187 motion photogrammetry with geospatial software as a novel technique for quantifying 3D
 1188 ecological characteristics of coral reefs, *PeerJ*, 3, doi:10.7717/peerj.1077, 2015.

1189 Castillo, C., Pérez, R., James, M. R., Quinton, J. N., Taguas, E. V. and Gómez, J. A.:
 1190 Comparing the Accuracy of Several Field Methods for Measuring Gully Erosion, *Soil Sci.*
 1191 *Soc. Am. J.*, 76, doi:10.2136/sssaj2011.0390, 2012.

1192 Castillo, C., Taguas, E. V., Zarco-Tejada, P., James, M. R. and Gómez, J. A.: The normalized
 1193 topographic method: an automated procedure for gully mapping using GIS, *Earth Surf. Proc.*
 1194 *Landf.*, 39, 2002–2015, doi:10.1002/esp.3595, 2014.

1195 Castillo, C., James, M. R., Redel-Macías, M. D., Pérez, R. and Gómez, J. A.: SF3M software:
 1196 3-D photo-reconstruction for non-expert users and its application to a gully network, *SOIL*, 1,
 1197 583–594, doi:10.5194/soil-1-583-2015, 2015.

1198 Cavalli, M., Tarolli, P., Marchi, L. and Fontana, G. D.: The effectiveness of airborne LiDAR
 1199 data in the recognition of channel-bed morphology, *Catena*, 73(3), 249–260,
 1200 doi:10.1016/j.catena.2007.11.001, 2008.

1201 Chandler, J.: Effective application of automated digital photogrammetry for
 1202 geomorphological research, *Earth Surf. Proc. Landf.*, 24, 51–63, 1999.

1203 Chen, L. C., Lo, C. Y., Liu, C. L. And Chen, A. J.: Orientation modelling by matching image
 1204 templates of a GCP database, *Proc. 21st ACRS*, 21(2), 2000.

1205 Cignoni, P., Callieri, M., Corsini, M., Dellepiane, M., Ganovelli, F. And Ranzuglia, G.:
 1206 MeshLab: an Open-Source Mesh Processing Tool, in: *Eurographics Italian Chapter*
 1207 *Conference*, Salerno, Italy, 129–136, 2008.

1208 Clapuyt, F., Vanacker, V. and Van Oost, K.: Reproducibility of UAV-based earth topography
 1209 reconstructions based on Structure-from-Motion algorithms, *Geomorphology*,
 1210 doi:10.1016/j.geomorph.2015.05.011, 2015.

1211 Collier, P.: The impact on topographic mapping of developments in land and air survey:
 1212 1900-1939, *Cartogr. Geogr. Inform.*, 29(3), 155-174, 2002.

1213 Dall'Asta, E., Delaloye, R., Diotri, F., Forlani, G., Fornari, Morro di Cella, U. M.,
 1214 Pogliotti, P., Roncella, R. and Santise, M.: Use of UAS in a High Mountain Landscape: the
 1215 Case of Gran Sommetta Rock Glacier (AO). *ISPRS – Int. Arch. Photogramm. Rem. Sens.*,
 1216 XL-3/W3, 391-397, 2015.

1217 Dandois, J. P. and Ellis, E. C.: High spatial resolution three-dimensional mapping of
 1218 vegetation spectral dynamics using computer vision, *Remote Sens. Environ.*, 136, 259–276,
 1219 doi:10.1016/j.rse.2013.04.005, 2013.

1220 Díaz-Varela, R., de la Rosa, R., León, L. and Zarco-Tejada, P.: High-Resolution Airborne
 1221 UAV Imagery to Assess Olive Tree Crown Parameters Using 3D Photo Reconstruction:
 1222 Application in Breeding Trials, *Remote Sensing*, 7, 4213–4232. doi:10.3390/rs70404213,
 1223 2015.

1224 Dietrich, J. T.: Riverscape Mapping with Helicopter-Based Structure-From-Motion
1225 Photogrammetry, *Geomorphology*, 252, 144–157, doi:10.1016/j.geomorph.2015.05.008,
1226 2016.

1227 Doyle, F.: The Historical Development of Analytical Photogrammetry. *Photogrammetric*
1228 *Engineering*, 15(2), 259-265, 1964.

1229 Ducher, G.: Photogrammetry - The largest operational application of remote sensing,
1230 *Photogrammetria*, 41(2), 72-82., 1987.

1231 East, A. E., Pess, G. R., Bountry, J. A., Magirl, C. S., Ritchie, A. C., Logan, J. B., Randle, T.
1232 J., Mastin, M. C., Minear, J. T., Duda, J. J., Liermann, M. C., McHenry, M. L., Beechie, T. J.
1233 and Shafroth, P. B.: Reprint of: Large-scale dam removal on the Elwha River, Washington,
1234 USA: River channel and floodplain geomorphic change, *Geomorphology*, 246, 687–708,
1235 doi:10.1016/j.geomorph.2015.04.027, 2015.

1236 Eling, C., Wieland, M., Hess, C., Klingbeil, L. and Kuhlmann, H.: Development and
1237 evaluation of a UAV based mapping system for remote sensing and surveying applications,
1238 *ISPRS – Int. Arch. Photogramm. Rem. Sens.*, XL-1/W4, 233-239, 2015.

1239 Eltner, A., Mulsow, C. and Maas, H.: Quantitative Measurement of Soil Erosion from TIs and
1240 Uav Data, *ISPRS - Int. Arch. Photogramm. Rem. Sens.*, XL-1/W2, 119–124, 2013.

1241 Eltner, A. and Baumgart, P.: Accuracy constraints of terrestrial Lidar data for soil erosion
1242 measurement: Application to a Mediterranean field plot, *Geomorphology*, 245, 243–254,
1243 doi:10.1016/j.geomorph.2015.06.008, 2015.

1244 Eltner, A., Baumgart, P., Maas, H.-G. and Faust, D.: Multi-temporal UAV data for automatic
1245 measurement of rill and interrill erosion on loess soil. *Earth Surf. Proc. Landf.*, 40(6), 741–
1246 755, doi:10.1002/esp.3673, 2015.

1247 Eltner, A. and Schneider, D.: Analysis of Different Methods for 3D Reconstruction of Natural
1248 Surfaces from Parallel-Axes UAV Images, *Photogramm. Rec.*, 30(151), 279–299,
1249 doi:10.1111/phor.12115, 2015.

1250 Favalli, M., Fornaciai, A., Isola, I., Tarquini, S. and Nannipieri, L.: Multiview 3D
1251 reconstruction in geosciences, *Comput. Geosc.*, 44, 168–176,
1252 doi:10.1016/j.cageo.2011.09.012, 2012.

1253 Fekete, S., Diederichs, M. and Lato, M.: Geotechnical and operational applications for 3-
1254 dimensional laser scanning in drill and blast tunnels, *Tunnelling and Underground Space*
1255 *Technology*, 25(5), 614–628, doi:10.1016/j.tust.2010.04.008, 2010.

1256 Fernández, T., Pérez, J. L., Cardenal, F. J., López, A., Gómez, J. M., Colomo, C., Delgado, J.
1257 and Sánchez, M.: Use of a Light UAV and Photogrammetric Techniques To Study the
1258 Evolution of a Landslide in Jaén (Southern Spain), *ISPRS – Int. Arch. Photogramm. Rem.*
1259 *Sens.*, XL-3/W3, 241–248, doi:10.5194/isprsarchives-XL-3-W3-241-2015, 2015.

1260 Fonstad, M. A., Dietrich, J. T., Courville, B. C., Jensen, J. L. and Carbonneau, P. E.:
1261 Topographic structure from motion: a new development in photogrammetric measurement,
1262 *Earth Surf. Proc. Landf.*, 38, 421–430, doi:10.1002/esp.3366, 2013.

1263 Frahm, J.-M., Pollefeys, M., Lazebnik, S., Gallup, D., Clipp, B., Raguram, R., Wu, C., Zach,
1264 C. and Johnson, T.: Fast robust large-scale mapping from video and internet photo
1265 collections., *ISPRS J. Photogramm.*, 65(6), 538–549, doi:10.1016/j.isprsjprs.2010.08.009,
1266 2010.

1267 Franceschi, M., Teza, G., Preto, N., Pesci, A., Galgaro, A. and Girardi, S.: Discrimination
1268 between marls and limestones using intensity data from terrestrial laser scanner, *ISPRS J.*
1269 *Photogramm.*, 64(6), 522–528, doi:10.1016/j.isprsjprs.2009.03.003, 2009.

1270 Francioni, M., Salvini, R., Stead, D., Giovannini, R., Riccucci, S., Vanneschi, C. and Gulli,
1271 D.: An integrated remote sensing-GIS approach for the analysis of an open pit in the Carrara
1272 marble district, Italy: Slope stability assessment through kinematic and numerical methods,
1273 *Comp. Geot.*, 67, 46–63, doi:10.1016/j.compgeo.2015.02.009, 2015.

1274 Frankl, A., Stal, C., Abraha, A., Nyssen, J., Rieke-Zapp, D., De Wulf, A. and Poesen, J.:
1275 Detailed recording of gully morphology in 3D through image-based modelling PhotoScan
1276 Digital Elevation Model (DEM) Soil pipes Structure from Motion–Multi View Stereo
1277 (SfM–MVS) Volume calculation, *Catena*, 127, 92–101, doi:10.1016/j.catena.2014.12.016,
1278 2014.

1279 Fugazza, D., Senese, A., Azzoni, R. S., Smiraglia, C. Cernuschi, M. Severi, D. D. and
1280 Guglielmina, A.: High-resolution mapping of glacier surface features. The UAV survey of the
1281 Forni glacier (Stelvio National Park, Italy), *Geogr. Fis. Dinam. Quat.*, 38, 25–33,
1282 doi:10.4461/GFDQ.2015.38.03, 2015.

1283 Furukawa, Y., Curless, B., Seitz, S. M. and Szeliski, R.: Towards Internet-scale multi-view
1284 stereo, in: IEEE Conference on Computer Vision and Pattern Recognition, San Francisco,
1285 CA, USA, 1434–1441, doi:10.1109/CVPR.2010.5539802, 2010.

1286 Furukawa, Y. and Ponce, J.: Accurate, dense, and robust multiview stereopsis, in: IEEE
1287 Transactions on Pattern Analysis and Machine Intelligence, 83, 1362–1376,
1288 doi:10.1109/TPAMI.2009.161, 2010.

1289 Genchi, S. A., Vitale, A. J., Perillo, G. M. E. and Delrieux, C. A.: Structure-from-Motion
1290 Approach for Characterization of Bioerosion Patterns Using UAV Imagery, Sensors, 15,
1291 3593–3609, doi:10.3390/s150203593, 2015.

1292 Gienko, G. A. and Terry, J. P.: Three-dimensional modeling of coastal boulders using multi-
1293 view image measurements, Earth Surf. Proc. Landf., 39, 853–864, doi:10.1002/esp.3485,
1294 2014.

1295 Gigli, G. and Casagli, N.: Semi-automatic extraction of rock mass structural data from high
1296 resolution LIDAR point clouds., Int. J. Rock Mech. Min., 48, 187–198,
1297 doi:10.1016/j.ijrmms.2010.11.009, 2011.

1298 Girardeau-Montaut, D.: CloudCompare (version 2.x; GPL software), EDF RandD, Telecom
1299 ParisTech, <http://www.cloudcompare.org/>, last access: Mar. 2015.

1300 Gomez, C.: Digital photogrammetry and GIS-based analysis of the bio-geomorphological
1301 evolution of Sakurajima Volcano, diachronic analysis from 1947 to 2006. J. Volcanol. Geoth.,
1302 280, 1–13, 2014.

1303 Gomez, C., Hayakawa, Y. and Obanawa, H.: A study of Japanese landscapes using structure
1304 from motion derived DSMs and DEMs based on historical aerial photographs: New opportu-
1305 nities for vegetation monitoring and diachronic geomorphology, Geomorphology, 242, 11–20,
1306 doi:10.1016/j.geomorph.2015.02.021, 2015.

1307 Gómez-Gutiérrez, Á., de Sanjosé-Blasco, J. J., de Matías-Bejarano, J. and Berenguer-
1308 Sempere, F.: Comparing Two Photo-Reconstruction Methods to Produce High Density Point
1309 Clouds and DEMs in the Corral del Veleta Rock Glacier (Sierra Nevada, Spain), Remote
1310 Sensing, 6, 5407–5427, doi:10.3390/rs6065407, 2014.

1311 Gómez-Gutiérrez, Á., Schnabel, S., Berenguer-Sempere, F., Lavado-Contador, F. and Rubio-
1312 Delgado, J.: Using 3D photo-reconstruction methods to estimate gully headcut erosion,
1313 Catena, 120, 91–101, doi:10.1016/j.catena.2014.04.004, 2014.

1314 Gómez-Gutiérrez, Á., de Sanjosé-Blasco, J., Lozano-Parra, J., Berenguer-Sempere, F. and de
 1315 Matías-Bejarano, J.: Does HDR Pre-Processing Improve the Accuracy of 3D Models
 1316 Obtained by Means of two Conventional SfM-MVS Software Packages? The Case of the
 1317 Corral del Veleto Rock Glacier, *Remote Sensing*, 7, 10269–10294, doi:10.3390/rs70810269,
 1318 2015.

1319 Gruen, A.: Development and status of image matching in photogrammetry, *Photogramm.*
 1320 *Rec.*, 27(137), 36–57, doi:10.1111/j.1477-9730.2011.00671.x, 2012.

1321 Hartzell, P., Glennie, C., Biber, K., and Khan, S. (2014). Application of multispectral LiDAR
 1322 to automated virtual outcrop geology. *ISPRS Journal of Photogrammetry and Remote*
 1323 *Sensing*, 88, 147–155. doi:10.1016/j.isprsjprs.2013.12.004

1324 Harwin, S. and Lucieer, A.: Assessing the Accuracy of Georeferenced Point Clouds Produced
 1325 via Multi-View Stereopsis from Unmanned Aerial Vehicle (UAV) Imagery, *Remote Sensing*,
 1326 4, 1573–1599, doi:10.3390/rs4061573, 2012.

1327 Heritage, G. and Hetherington, D.: Towards a protocol for laser scanning in fluvial
 1328 geomorphology, *Earth Surf. Proc. Landf.*, 32(32), 66–74, doi:10.1002/esp.1375, 2007.

1329 Hirschmüller, H.: Semi-Global Matching – Motivation, Developments and Applications,
 1330 *Photogrammetric Week*, 11, 173–184, 2011.

1331 Humair, F., Abellan, A., Carrea, D., Matasci, B., Epard, J.-L. and Jaboyedoff, M.: Geological
 1332 layers detection and characterisation using high resolution 3D point clouds: example of a box-
 1333 fold in the Swiss Jura Mountains, *Eur. J. Rem. Sens.*, 48, 541–568,
 1334 doi:10.5721/EuJRS20154831, 2015.

1335 Immerzeel, W. W., Kraaijenbrink, A., Shea, J. M., Shrestha, A. B., Pellicciotti, F., Bierkens,
 1336 M. F. P. and De Jong, S. M.: High-resolution monitoring of Himalayan glacier dynamics
 1337 using unmanned aerial vehicles, *Rem. Sens. Environ.*, 150, 93–103,
 1338 doi:10.1016/j.rse.2014.04.025, 2014.

1339 Jaboyedoff, M., Metzger, R., Oppikofer, T., Couture, R., Derron, M.-H., Locat, J. and Turmel,
 1340 D.: New insight techniques to analyze rock-slope relief using DEM and 3D- imaging cloud
 1341 points: COLTOP-3D software. In: *Rock Mechanics: Meeting Society's Challenges and*
 1342 *Demands*, Eberhardt, E., Stead, D. and Morrison, T. (Eds.), 1st ed., Taylor and Francis,
 1343 London, 61–68, 2007.

1344 Jaboyedoff, M., Oppikofer, T., Abellán, A., Derron, M.-H., Loye, A., Metzger, R. and
 1345 Pedrazzini, A.: Use of LIDAR in landslide investigations: a review, *Nat. Hazards*, 61, 5-28,
 1346 doi: 10.1007/s11069-010-9634-2, 2012.

1347 Jackson, M. and Magro, G.: Real-time crowd-sourcing, data and modelling. In: *IAIA15*
 1348 *Conference Proceedings*, Florence, 2015.

1349 James, M. R. and Robson, S.: Straightforward reconstruction of 3D surfaces and topography
 1350 with a camera: Accuracy and geoscience application, *J. Geoph. Res.*, 117, F03017,
 1351 doi:10.1029/2011JF002289, 2012.

1352 James, M. R. and Varley, N.: Identification of structural controls in an active lava dome with
 1353 high resolution DEMs: Volcán de Colima, Mexico, *Geoph. Res. Let.*, 39, L22303,
 1354 doi:10.1029/2012GL054245, 2012.

1355 James, M. R. and Robson, S.: Mitigating systematic error in topographic models derived from
 1356 UAV and ground-based image networks, *Earth Surf. Proc. Landf.*, 39, 1413–1420,
 1357 doi:10.1002/esp.3609, 2014.

1358 James, M. R. and Robson, S.: Sequential digital elevation models of active lava flows from
 1359 ground-based stereo time-lapse imagery, *ISPRS J. Photogramm. Rem. Sens.*, 97, 160–170,
 1360 doi:10.1016/j.isprsjprs.2014.08.011, 2014.

1361 Javernick, L., Brasington, J. and Caruso, B.: Modeling the topography of shallow braided
 1362 rivers using Structure-from-Motion photogrammetry, *Geomorphology*, 213, 166–182,
 1363 doi:10.1016/j.geomorph.2014.01.006, 2014.

1364 Johnson, K., Nissen, E., Saripalli, S., Arrowsmith, J. R., McGarey, P., Scharer, K., Williams,
 1365 P. and Blisniuk, K.: Rapid mapping of ultrafine fault zone topography with structure from
 1366 motion, *Geosphere*, 10(5), doi:10.1130/GES01017.1, 2014.

1367 Johnson-Roberson, M., Bryson, M., Douillard, B., Pizarro, O. and Williams, S. B.:
 1368 Discovering salient regions on 3D photo-textured maps: Crowdsourcing interaction data from
 1369 multitouch smartphones and tablets, *Comput. Vis. Image Und.*, 131, 28–41,
 1370 doi:10.1016/j.cviu.2014.07.006, 2015.

1371 Kääb, A.: Glacier Volume Changes Using ASTER Satellite Stereo and ICESat GLAS Laser
 1372 Altimetry. A Test Study on Edgeøya, Eastern Svalbard, *IEEE Transactions on Geoscience*
 1373 *and Remote Sensing*, 46(10), 2823 – 2830, doi:10.1109/TGRS.2008.2000627, 2008.

1374 Kääb, A., Girod, L. and Berthling, I.: Surface kinematics of periglacial sorted circles using
1375 structure-from-motion technology, *The Cryosphere*, 8, 1041–1056, doi:10.5194/tc-8-1041-
1376 2014, 2014.

1377 Kaiser, A., Neugirg, F., Rock, G., Müller, C., Haas, F., Ries, J., and Schmidt, J.: Small-Scale
1378 Surface Reconstruction and Volume Calculation of Soil Erosion in Complex Moroccan Gully
1379 Morphology Using Structure from Motion, *Remote Sensing*, 6, 7050–7080,
1380 doi:10.3390/rs6087050, 2014.

1381 Kaiser, A., Neugirg, F., Haas, F., Schmidt, J., Becht, M. and Schindewolf, M.: Determination
1382 of hydrological roughness by means of close range remote sensing, *SOIL*, 1, 613–620,
1383 doi:10.5194/soil-1-613-2015, 2015.

1384 Khoshelham, K., Altundag, D., Ngan-Tillard, D. and Menenti, M.: Influence of range
1385 measurement noise on roughness characterization of rock surfaces using terrestrial laser
1386 scanning, *Int. J. Rock Mech. Min.*, 48, 1215–1223, doi:10.1016/j.ijrmms.2011.09.007, 2011.

1387 Kraus, K.: *Photogrammetry: Geometry from Images and Laser Scans*, 2nd edition, De
1388 Gruyter, Berlin, Germany, 459 pages, 2007.

1389 Kromer, R., Abellán, A., Hutchinson, D., Lato, M., Edwards, T. and Jaboyedoff, M.: A 4D
1390 Filtering and Calibration Technique for Small-Scale Point Cloud Change Detection with a
1391 Terrestrial Laser Scanner, *Remote Sensing*, 7(10), 13029–13052, doi:10.3390/rs71013029,
1392 2015.

1393 Lague, D., Brodu, N., and Leroux, J.: Accurate 3D comparison of complex topography with
1394 terrestrial laser scanner: Application to the Rangitikei canyon (N-Z), *ISPRS J. Photogramm.*
1395 *Rem. Sens.*, 82, 10–26, doi:10.1016/j.isprsjprs.2013.04.009, 2013.

1396 Laussedat, A.: *La métrophotographie*, Bibliothèque Photographique, Gauthier-Villars, Paris,
1397 55 pages, 1899.

1398 Lato, M., Hutchinson, J., Diederichs, M., Ball, D. and Harrap, R.: Engineering monitoring of
1399 rockfall hazards along transportation corridors: using mobile terrestrial LiDAR, *Nat. Hazard*
1400 *Earth Sys.*, 9, 935–946, 2009.

1401 Leon, J. X., Roelfsema, C. M., Saunders, M. I. and Phinn, S. R.: Measuring coral reef terrain
1402 roughness using “Structure-from-Motion” close-range photogrammetry, *Geomorphology*,
1403 242, 21–28, doi:10.1016/j.geomorph.2015.01.030, 2015.

1404 Lim, M., Petley, D. N., Rosser, N. J., Allison, R. J., Long, A. J. and Pybus, D.: Combined
 1405 digital photogrammetry and time-of-flight laser scanning for monitoring cliff evolution,
 1406 *Photogramm. Rec.*, 20(110), 109–129, 2008.

1407 [Lowe, D. G.: Object recognition from local scale-invariant features, The Proceedings of the](#)
 1408 [7th IEEE International Conference on Computer Vision, 2, 1150–1157, 1999.](#)

1409 Lucieer, A., de Jong, S. and Turner, D.: Mapping landslide displacements using Structure
 1410 from Motion (SfM) and image correlation of multi-temporal UAV photography, *Prog. Phys.*
 1411 *Geog.*, 38, 1–20, doi:10.1177/0309133313515293, 2013.

1412 Lucieer, A., Turner, D., King, D. H. and Robinson, S. A.: Using an unmanned aerial vehicle
 1413 (UAV) to capture micro-topography of antarctic moss beds, *Int. J. Appl. Earth Obs.*, 27, 53–
 1414 62, doi:10.1016/j.jag.2013.05.011, 2014.

1415 Luhmann, T., Robson, S., Kyle, S. and Boehm, J.: *Close-Range Photogrammetry and 3D*
 1416 *Imaging*, 2nd edition, De Gruyter, Berlin, Germany, 683 pages, 2014.

1417 Mancini, F., Dubbini, M., Gattelli, M., Stecchi, F., Fabbri, S. and Gabbianelli, G.: Using
 1418 Unmanned Aerial Vehicles (UAV) for High-Resolution Reconstruction of Topography: The
 1419 Structure from Motion Approach on Coastal Environments, *Remote Sensing*, 5, 6880–6898,
 1420 doi:10.3390/rs5126880, 2013.

1421 Martin-Brualla, R., Gallup, D. and Seitz, S. M.: Time-lapse Mining from Internet Photos. in:
 1422 *IEEE International Conference on Computer Vision (ICCV)*, 2015.

1423 Masiero, A., Guarnieri, A., Vettore, A. and Pirotti, F.: An ISVD-based Euclidian structure
 1424 from motion for smartphones, *Int. Arch. Photogramm. Rem. Sens.*, XL-5, 401-406, 2014.

1425 Meesuk, V., Vojinovic, Z., Mynett, A. E., and Abdullah, A. F.: Urban flood modelling
 1426 combining top-view LiDAR data with ground-view SfM observations, *Adv. Water Res.*, 75,
 1427 105–117, doi:10.1016/j.advwatres.2014.11.008, 2015.

1428 Micheletti, N., Chandler, J. H. and Lane, S. N.: Investigating the geomorphological potential
 1429 of freely available and accessible structure-from-motion photogrammetry using a smartphone,
 1430 *Earth Surf. Proc. Landf.*, 40, 473–486, doi:10.1002/esp.3648, 2014.

1431 Micheletti, N., Chandler, J. H. and Lane, S. N.: Structure from Motion (SfM)
 1432 Photogrammetry (Chap. 2, Sec. 2.2), In: Cook, S.J., Clarke L.E. and Nield, J.M. (Eds.)
 1433 *Geomorphological Techniques*, British Society of Geomorphology, London, 2015.

1434 Michoud, C., Carrea, D., Costa, S., Derron, M.-H., Jaboyedoff, M., Delacourt, C., Maquaire,
1435 O., Letortu, P. and Davidson, R.: Landslide detection and monitoring capability of boat-based
1436 mobile laser scanning along Dieppe coastal cliffs, Normandy, *Landslides*, 12(2), 403–418,
1437 2015.

1438 Mikhail, E., Bethel, J. and McGlone, J.: *Introduction to Modern Photogrammetry*, John Wiley
1439 and Sons, Inc., New York, 479 pages, 2001.

1440 Milan, D. J., Heritage, G. L. and Hetherington, D.: Assessment of erosion and deposition
1441 volumes and channel change Application of a 3D laser scanner in the assessment of erosion
1442 and deposition volumes and channel change in a proglacial river, *Earth Surf. Proc. Landf.*,
1443 32(32), 1657–1674, doi:10.1002/esp.1592, 2007.

1444 Monserrat, O. and Crosetto, M.: Deformation measurement using terrestrial laser scanning
1445 data and least squares 3D surface matching, *ISPRS J. Photogramm. Rem. Sens.*, 63(1), 142–
1446 154, doi:10.1016/j.isprsjprs.2007.07.008, 2008.

1447 Morgenroth, J. and Gomez, C.: Assessment of tree structure using a 3D image analysis
1448 technique—A proof of concept; *Urban Forestry and Urban Greening*, 13(1), 198–203,
1449 doi:10.1016/j.ufug.2013.10.005, 2014

1450 Nadal-Romero, E., Revuelto, J., Errea, P. and López-Moreno, J. I.: The application of
1451 terrestrial laser scanner and SfM photogrammetry in measuring erosion and deposition
1452 processes in two opposite slopes in a humid badlands area (central Spanish Pyrenees), *SOIL*,
1453 1, 561–573, doi:10.5194/soil-1-561-2015, 2015.

1454 Nolan, M., Larsen, C. and Sturm, M.: Mapping snow-depth from manned-aircraft on
1455 landscape scales at centimeter resolution using Structure-from-Motion photogrammetry, *The*
1456 *Cryosphere Disc.*, 9, 333–381, doi:10.5194/tcd-9-333-2015, 2015.

1457 Nouwakpo, S. K., James, M. R., Weltz, M. A., Huang, C.-H., Chagas, I. and Lima, L.:
1458 Evaluation of structure from motion for soil microtopography measurement, *Photogramm.*
1459 *Rec.*, 29(147), 297–316, doi:10.1111/phor.12072, 2014.

1460 Nouwakpo, S. K., Weltz, M. A. and McGwire, K.: Assessing the performance of Structure-
1461 from-Motion photogrammetry and terrestrial lidar for reconstructing soil surface
1462 microtopography of naturally vegetated plots, *Earth Surf. Proc. Landf.*, doi:10.1002/esp.3787,
1463 2015.

1464 Oppikofer, T., Jaboyedoff, M., Blikra, L., Derron, M.-H. and Metzger, R.: Characterization
 1465 and monitoring of the Aknes rockslide using terrestrial laser scanning, *Natural Hazards and*
 1466 *Earth System Sciences*, 9, 1003–1019, 2009.

1467 Ouédraogo, M. M., Degré, A., Debouche, C. and Lisein, J.: The evaluation of unmanned
 1468 aerial system-based photogrammetry and terrestrial laser scanning to generate DEMs of
 1469 agricultural watersheds, *Geomorphology*, 214, 339–355,
 1470 doi:10.1016/j.geomorph.2014.02.016, 2014.

1471 Passalacqua, P., Belmont, P., Staley, D. M., Simley, J. D., Arrowsmith, J. R., Bode, C. A.,
 1472 Crosby, C., DeLong, S. B., Glenn, N. F., Kelly, S. A., Lague, D., Sangireddy, H., Schaffrath,
 1473 K., Tarboton, D. G., Wasklewicz, T. and Wheaton, J. M.: Analyzing high resolution
 1474 topography for advancing the understanding of mass and energy transfer through landscapes:
 1475 A review. *Earth-Sci. Rev.*, 148, 174–193, doi:10.1016/j.earscirev.2015.05.012, 2015.

1476 Pears, N., Liu, Y. and Bunting, P.: *3D Imaging, Analysis and Applications*, Springer, London,
 1477 499 pages, 2012.

1478 Piermattei, L., Carturan, L. and Guarnieri, A.: Use of terrestrial photogrammetry based on
 1479 structure from motion for mass balance estimation of a small glacier in the Italian Alps, *Earth*
 1480 *Surf. Proc. Landf.*, 40(13), 1791–1802, doi:10.1002/esp.3756, 2015.

1481 Pierrot-Deseilligny, M. and Clery, I.: APERO, an open source bundle adjustment software for
 1482 automatic calibration and orientation of set of images, *Intern. Arch. Photogramm. Rem. Sens.*,
 1483 38-5(W16), 269–276, 2011.

1484 Pierrot-Deseilligny, M. and Clery, I.: Some possible protocols of acquisition for the optimal
 1485 use of the “Apero” open source software in automatic orientation and calibration, *EuroCow*
 1486 2012, Barcelona, Spain, (10pp), 2012.

1487 Pike, R. J., Evans, I. S. and Hengl, T.: Geomorphometry: a Brief Guide. In: Hengl, T. and
 1488 Reuter, H.I. (Eds) *Geomorphometry: Concepts, Software, Applications. Developments in Soil*
 1489 *Science*, 33, 1-28, 2008.

1490 Pollyea, R. and Fairley, J.: Estimating surface roughness of terrestrial laser scan data using
 1491 orthogonal distance regression, *Geology*, 39(7), 623–626, doi:10.1130/G32078.1, 2011.

1492 Poropat, G.: Measurement of Surface Roughness of Rock Discontinuities. In *Proc. of the 3rd*
 1493 *CANUS Rock Mechanics Symposium*. Toronto, 2009.

1494 Prosdocimi, M., Calligaro, S., Sofia, G., Dalla Fontana, G. and Tarolli, P.: Bank erosion in
1495 agricultural drainage networks: new challenges from Structure-from-Motion photogrammetry
1496 for post-event analysis, *Earth Surf. Proc. Landf.*, 40(14), 1891–1906, doi:10.1002/esp.3767,
1497 2015.

1498 Remondino, F., Spera, M. G., Nocerino, E., Menna, F. and Nex, F.: State of the art in high
1499 density image matching, *Photogramm. Rec.*, 29(146), 144–166, doi:10.1111/phor.12063,
1500 2014.

1501 Rippin, D. M., Pomfret, A. and King, N.: High resolution mapping of supraglacial drainage
1502 pathways reveals link between micro-channel drainage density, surface roughness and surface
1503 reflectance, *Earth Surf. Proc. Landf.*, 40(10), 1279–1290, doi:10.1002/esp.3719, 2015.

1504 Royan, M., Abellan, A. and Vilaplana, J.: Progressive failure leading to the 3 December 2013
1505 rockfall at Puigcercós scarp (Catalonia, Spain), *Landslides*, 12(3), 585–595, 2015.

1506 Ruzic, I., Marovic, I., Benac, C. and Ilic, S.: Coastal cliff geometry derived from structure-
1507 from-motion photogrammetry at Stara Baka, Krk Island, Croatia, *Geo-Mar. Lett.*, 34, 555–
1508 565, doi:10.1007/s00367-014-0380-4, 2014.

1509 Ryan, J. C., Hubbard, A. L., Box, J. E., Todd, J., Christoffersen, P., Carr, J. R., Holt, T. O.,
1510 and Snooke, N.: UAV photogrammetry and structure from motion to assess calving dynamics
1511 at Store Glacier, a large outlet draining the Greenland ice sheet, *The Cryosphere*, 9, 1–11,
1512 doi:10.5194/tc-9-1-2015, 2015.

1513 Sanz-Ablanedo, E., Rodríguez-Pérez, J. R., Armesto, J. and Taboada, M. F. Á.: Geometric
1514 stability and lens decentering in compact digital cameras, *Sensors*, 10, 1553–1572
1515 doi:10.3390/s100301553, 2010.

1516 Schaffalitzky, F. and Zisserman, A.: Multi-view matching for unordered image sets, or “How
1517 do I organize my holiday snaps?”, *Computer Vision - ECCV 2002*, 2350, 414–431.
1518 doi:10.1007/3-540-47969-4, 2002.

1519 Shortis, M. R., Bellman, C. J., Robson, S., Johnston, G. J. and Johnson, G. W.: Stability of
1520 Zoom and Fixed Lenses used with Digital SLR Cameras, *Intern. Arch. Photogramm., Rem.*
1521 *Sens.*, XXXVI(5), 285–290, 2006.

1522 Siebert, S. and Teizer, J.: Mobile 3D mapping for surveying earthwork projects using an
1523 Unmanned Aerial Vehicle (UAV) system, *Automation in Construction*, 41, 1–14,
1524 doi:10.1016/j.autcon.2014.01.004, 2014.

1525 Smith, M. W., Carrivick, J. L., Hooke, J. and Kirkby, M. J.: Reconstructing flash flood
1526 magnitudes using “Structure-from-Motion”: A rapid assessment tool, *J. Hydrol.*, 519, 1914–
1527 1927, doi:10.1016/j.jhydrol.2014.09.078, 2014.

1528 Smith, M. W. and Vericat, D.: From experimental plots to experimental landscapes:
1529 topography, erosion and deposition in sub-humid badlands from Structure-from-Motion
1530 photogrammetry, *Earth Surf. Proc. Landf.*, 40(12), 1656–1671, doi:10.1002/esp.3747, 2015.

1531 Smith, M. W., Carrivick, J. L. and Quincey, D. J.: Structure from motion photogrammetry in
1532 physical geography, *Progress in Physical Geography*, 1-29, doi: 10.1177/0309133315615805,
1533 2015.

1534 Snapir, B., Hobbs, S. and Waine, T. W.: Roughness measurements over an agricultural soil
1535 surface with Structure from Motion, *ISPRS J. Photogramm. Rem. Sens.*, 96, 210–223,
1536 doi:10.1016/j.isprsjprs.2014.07.010, 2014.

1537 Snavely, N., Seitz, S. M. and Szeliski, R.: Photo Tourism : Exploring Photo Collections in 3D,
1538 *ACM Transactions on Graphics*, 25(3), 835–846, 2006.

1539 Snavely, N., Seitz, S. M. and Szeliski, R.: Modeling the World from Internet Photo
1540 Collections, *Intern. J. Comput. Vis.*, 80(2), 189–210. doi:10.1007/s11263-007-0107-3, 2008.

1541 Stöcker, C., Eltner, A. and Karrasch, P.: Measuring gullies by synergetic application of UAV
1542 and close range photogrammetry — A case study from Andalusia, Spain, *Catena*, 132, 1–11,
1543 doi:10.1016/j.catena.2015.04.004, 2015.

1544 Stumpf, A., Malet, J.-P., Allemand, P., Pierrot-Deseilligny, M. and Skupinski, G.: Ground-
1545 based multi-view photogrammetry for the monitoring of landslide deformation and erosion,
1546 *Geomorphology*, 231, 130–145, doi:10.1016/j.geomorph.2014.10.039, 2014.

1547 Sturzenegger, M. and Stead, D.: Close-range terrestrial digital photogrammetry and terrestrial
1548 laser scanning for discontinuity characterization on rock cuts, *Eng. Geol.*, 106, 163–182,
1549 doi:10.1016/j.enggeo.2009.03.004, 2009.

1550 Tamminga, A. D., Eaton, B. C. and Hugenholtz, C. H.: UAS-based remote sensing of Wuvial
1551 change following an extreme Wood event, *Earth Surf. Proc. Landf.*, 40(11), 1464–1476,
1552 doi:10.1002/esp.3728, 2015.

1553 Thomsen, L., Stolte, J., Baartman, J. and Starkloff, T.: Soil roughness : comparing old and
1554 new methods and application in a soil erosion model, *SOIL*, 1, 399–410, doi:10.5194/soil-1-
1555 399-2015, 2015.

1556 Tonkin, T. N., Midgley, N. G., Graham, D. J. and Labadz, J. C.: The potential of small
 1557 unmanned aircraft systems and structure-from-motion for topographic surveys: A test of
 1558 emerging integrated approaches at Cwm Idwal, North Wales, *Geomorphology*, 226, 35–43,
 1559 doi:10.1016/j.geomorph.2014.07.021, 2014.

1560 Torres-Sánchez, J., López-Granados, F., Serrano, N., Arquero, O. and Peña, J. M.: High-
 1561 Throughput 3-D Monitoring of Agricultural-Tree Plantations with Unmanned Aerial Vehicle
 1562 (UAV) Technology, *PLOS One*, 10(6), doi:10.1371/journal.pone.0130479, 2015.

1563 Triggs, B., McLauchlan, P., Hartley, R. and Fitzgibbon, A.: Bundle Adjustment - A Modern
 1564 Synthesis. In: Triggs, B., Zisserman, A. and Szeliski, R. (Eds.), *Vision Algorithms: Theory
 1565 and Practice*, Springer, Berlin, Germany, LNCS vol. 1883, 298–372, 2000.

1566 Turner, D., Lucieer, A. and de Jong, S.: Time Series Analysis of Landslide Dynamics Using
 1567 an Unmanned Aerial Vehicle (UAV), *Remote Sensing*, 7, 1736–1757,
 1568 doi:10.3390/rs70201736, 2015.

1569 Ullman, S.: The interpretation of structure from motion. *Proceedings of the Royal Society B*,
 1570 203, 405–426, 1979.

1571 Vasuki, Y., Holden, E. J., Kovesi, P. and Micklethwaite, S.: Semi-automatic mapping of
 1572 geological Structures using UAV-based photogrammetric data: An image analysis approach,
 1573 *Comput. Geosci.*, 69, 22–32, doi:10.1016/j.cageo.2014.04.012, 2014.

1574 Westoby, M. J., Brasington, J., Glasser, N. F., Hambrey, M. J. and Reynolds, J. M.:
 1575 “Structure-from-Motion” photogrammetry: A low-cost, effective tool for geoscience
 1576 applications, *Geomorphology*, 179, 300–314, doi:10.1016/j.geomorph.2012.08.021, 2012.

1577 Westoby, M. J., Glasser, N. F., Hambrey, M. J., Brasington, J., Reynolds, J. M. and Hassan,
 1578 M. A. A. M.: Reconstructing historic glacial lakeoutburst floods through numerical modelling
 1579 and geomorphological assessment: Extreme events in the Himalaya, *Earth Surf. Proc. Landf.*,
 1580 39, 1675–1692, doi:10.1002/esp.3617, 2014.

1581 Woodget, A. S., Carboneau, P. E., Visser, F. and Maddock, I. P.: Quantifying submerged
 1582 fluvial topography using hyperspatial resolution UAS imagery and structure from motion
 1583 photogrammetry, *Earth Surf. Proc. Landf.*, 40(1), 47–64, doi:10.1002/esp.3613, 2015.

1584 Wu, C.: Towards linear-time incremental structure from motion, in: *International Conference
 1585 on 3D Vision - 3DV*, Seattle, WA, USA, 127–134, 2013.

1586 Wu, C.: Critical configurations for radial distortion self-calibration, in: IEEE Conference on
1587 Computer Vision and Pattern Recognition (CVPR), 25 – 32. doi:10.1109/CVPR.2014.11,
1588 2014.

1589 Zarco-Tejada, P. J., Diaz-Varela, R., Angileri, V. and Loudjani, P.: Tree height quantification
1590 using very high resolution imagery acquired from an unmanned aerial vehicle (UAV) and
1591 automatic 3D photo-reconstruction methods, Eur. J. Agron., 55, 89–99,
1592 doi:10.1016/j.eja.2014.01.004, 2014.

1593

1594

1595 Table 1. Nomenclature and brief definitions of image-based 3D reconstruction related terms

Image-based 3D reconstruction	recording of the three-dimensional shape of an object from overlapping images from different perspectives
Computer Vision	algorithmic efforts to imitate human vision with focus on automation, amongst others, to reconstruct 3D scenes with methods of image processing and image understanding
Structure from Motion (SfM)	fully automatic reconstruction of 3D scenes from 2D images and simultaneous retrieval of the corresponding camera geometry in an arbitrary coordinate system
Photogrammetry	algorithmic efforts to determine 3D model coordinates and camera geometry focussing on accuracy and precise measurement in images
SfM photogrammetry	fully automatic reconstruction of 3D scenes from 2D images and camera geometry with option to set parameters for (photogrammetric) optimisation of accuracy and precision
Dense matching	increase of resolution of point clouds that model 3D scenes by pixel- or patch-wise matching in images of known intrinsic and extrinsic parameters
Stereo matching	reconstruction of object point through matching (in image space, Remondino et al., 2014) between two overlapping images
Multi-View-Stereo (MVS) matching	reconstruction of object point through matching (in object space, Remondino et al., 2014) from multiple overlapping images
Extrinsic parameters	exterior camera geometry comprising position (three shifts) and orientation (three rotations) of the camera projection centre
Intrinsic parameters	interior camera geometry comprising principle distance (distance between projection centre and image sensor), principle point (intersection of perpendicular from projection centre onto image plane) and distortion parameters (e.g. radial distortion)
Bundle adjustment (BA)	least-square optimisation to simultaneously solve for extrinsic (and intrinsic) parameters of all images; the term bundle correlates to rays that derive from 3D points, converge in corresponding projection centres and intersect with image sensor
Camera self-calibration	intrinsic camera parameters are included as additional unknowns into BA to solve for interior camera geometry
Ground Control Point (GCP)	in images clearly distinguishable point whose object coordinates are known to geo-reference surface model
Digital Elevation Model (DEM)	3D description of the surface in either raster (grid) or vector (mesh) format
Point cloud	quantity of points of 3D coordinates describing the surface within arbitrary or geo-referenced coordinate system, additional information such as normals or colours possible

1597 Table 2: Summary of non-commercial software tools beneficial for SfM photogrammetry processing and post-processing.

	Software	Bundler	PMVS2	Apero+ MicMac	SfMToolkit	Meshlab	Cloud Compare	Sfm_georef	VisualSfM	SF3M	Photosynth	123D Catch
	Type	Open Source	Open Source	Open Source	Open Source	Open Source	Open Source	Freely- available	Freely- available	Freely- available	Free web service	Free web service
	Website	http://www.cs.cornell.edu/~snaveily/bundler	http://www.dti.ens.fr/pmvs	http://logiciel.s.ign.fr/?Micmac	http://www.visual-experiments.com/demos/sfmtoolkit	http://meshlab.sourceforge.net	http://www.danielgm.net/cc	http://www.lancaster.ac.uk/staff/jamesm/software/sfm_georef.htm	http://ccwu.me/vsfm	http://sf3map.p.csic.es	https://photosynth.net	http://www.123dapp.com/catch
	Operative system	Linux Windows	Linux Windows	Linux Mac Windows	Windows	Mac Windows	Linux Mac Windows	Windows	Linux Mac Windows	Windows	Windows	Windows Mac
Functionalities	Camera calibration			x								
	Bundle adjustment	x			x				x	x	x	x
	Bundle adjustment with GCPs			x								
	Sparse 3D reconstruction	x		x	x				x	x	x	x
	Geo-referencing			x				x	x	x		
	Dense 3D reconstruction		x	x					x	x		x
	Post-processing			x						x		
	Advanced cloud processing					x	x					

1598 Table 3: Key developments of SfM photogrammetry towards a standard tool in
1599 geomorphometry

1600
1601

key developments	authors
method introduction	James & Robson (2012), Westoby et al. (2012), Fonstad et al. (2013)
evaluation of accuracy potential	James & Robson (2012), Westoby et al. (2012), Castillo et al. (2012)
SfM with terrestrial images	James & Robson (2012), Westoby et al. (2012), Castillo et al. (2012)
SfM with UAV images	Harwin & Lucieer (2012)
application with mm resolution	Bretar et al. (2013), Snapir et al. (2014)
application covering km ²	Immerzeel et al. (2014)
mitigation of systematic errors (i.e. dome)	James & Robson (2014a), Eltner & Schneider (2015)
influence of image network geometry	Stumpf et al. (2014) , Micheletti et al. (2014), Piermattei et al. (2015)
usage of Smartphone for data acquisition	Micheletti et al. (2014)
time-lapse implementation	James & Robson (2014b)
influence of scale	Smith & Vericat (2015)
comparing tools and cameras	Stumpf et al. (2014) , Eltner & Schneider (2015)
<u>comparing cameras</u>	<u>Eltner & Schneider (2015)</u> , <u>Prosdocimi et al. (2015)</u>
synergetic usage of terrestrial and aerial images	Stöcker et al. (2015)
sub-merged topography	Woodget et al. (2015)
under water application	Leon et al. (2015)
<u>multi-temporal application</u>	<u>James & Varley (2012)</u> , <u>Lucieer et al. (2013)</u>
reuse of historical images	Gomez et al. (2015)

1602

Formatierte Tabelle

1603 Table 4. Overview of the publication history divided in the main topics from 2012 until
1604 editorial deadline in Nov. 2015. Several publications examined more than one topic resulting
1605 in a larger number of topics than actual publications (number in brackets in last row). IDs
1606 refer to the table in appendix A1.

Topic	2012	2013	2014	2015	2016	ID	Total number of publicatio ns on the respective topic
Soil science/erosi on	1	-	5	9	-	1, 2, 3, 5, 6, 9, 11, 18, 22, 23, 30, 31, 55, 60, 61	15
Volcanology	3	1	1	1	-	7, 15, 43, 44, 52, 54	6
Glaciology	-	-	4	6	-	12, 13, 14, 25, 27, 34, 37, 47, 51, 62	10
Mass movements	-	1	1	3	-	32, 35, 49, 56, 64	5
Fluvial morphology	-	1	5	3	1	4, 8, 16, 17, 21, 26, 29, 33, 37, 38	10
Coastal morphology	3	1	3	-	-	8 5, 20, 28, 36, 42, 50, 53	9 7

Formatiert: Keine, Abstand Vor: 1.2
Zeile, Keine Aufzählungen oder
Nummerierungen, Vom nächsten
Absatz trennen

1607
1608
1609
1610
1611

Others	1 10 2 11 8 12 5 13 - 14 7, 15 16												10, 17, 19, 24, 39, 40, 41, 45, 46, 48, 57, 58, 59, 63, 65	
	16	Topic	17	8	18	6	19	2	20	2	21	1(22	69
s (publications)														(65)

Formatiert: Keine, Abstand Vor: 1.2 Zeile, Keine Aufzählungen oder Nummerierungen, Vom nächsten Absatz trennen

Formatiert: Links, Keine, Abstand Vor: 1.2 Zeile, Keine Aufzählungen oder Nummerierungen, Vom nächsten Absatz trennen

Formatiert: Keine, Abstand Vor: 1.2 Zeile, Keine Aufzählungen oder Nummerierungen, Vom nächsten Absatz trennen

Formatiert: Keine, Abstand Vor: 1.2 Zeile, Keine Aufzählungen oder Nummerierungen, Vom nächsten Absatz trennen

1612 Table 5: Data acquisition and error assessment protocol for SfM photogrammetry;
 1613 independent from individual study design.

in the field:					
target specifics	study area extent		ground control specifics	GCP measurement (total station, GPS, ...)	
	sensor to surface distance			GCP description	
	ground sampling distance			GCP number	
	target complexity			GCP accuracy	
camera specifics	camera name		image acquisition specifics	illumination condition	
	camera type (SLR, CSC, ...)			image number	
	lens type (zoom - fixed)			image overlap	
	sensor resolution			base (distance between images)	
	sensor size			network configuration (conv. - parallel-axis)	
	pixel size			perspective (aerial - terrestrial)	
	focal length			notes	
	at the office:				
data processing specifics	SfM tool		accuracy assessment	registration residual	
	GCP integration (1-/2-staged)			reference type (LiDAR, RTK pts, ...)	
	output data type			reference error	
error ratios	relative error			error measure (M3C2, raster difference, ...)	
	reference superiority			statistical value (RMSE, std dev, ...)	
	theoretical error ratio		notes		

1614

1615 Figure captions

1616

1617 Figure 1: Schematic illustration of the versatility of SfM photogrammetry.

1618

1619 Figure 2. Map of the research sites of all studies of this review.

1620

1621 Figure 3. Variety of SfM photogrammetry tools used in the 65 reviewed studies.

1622

1623 Figure 4. Boxplots summarizing statistics: a) of the scale of the study reaches (N: 56; ID 1-3
1624 and 5-39 in Appendix A), b) the relative error (calculated in regard to distance and measured
1625 error, N: 54; ID 1-3, 5-12 and 14-39 in Appendix A), and c) the reference superiority
1626 (calculated in regard to measured error and reference error, N: 33; ID 1-30 and 32-39 in
1627 Appendix A) of reviewed studies.

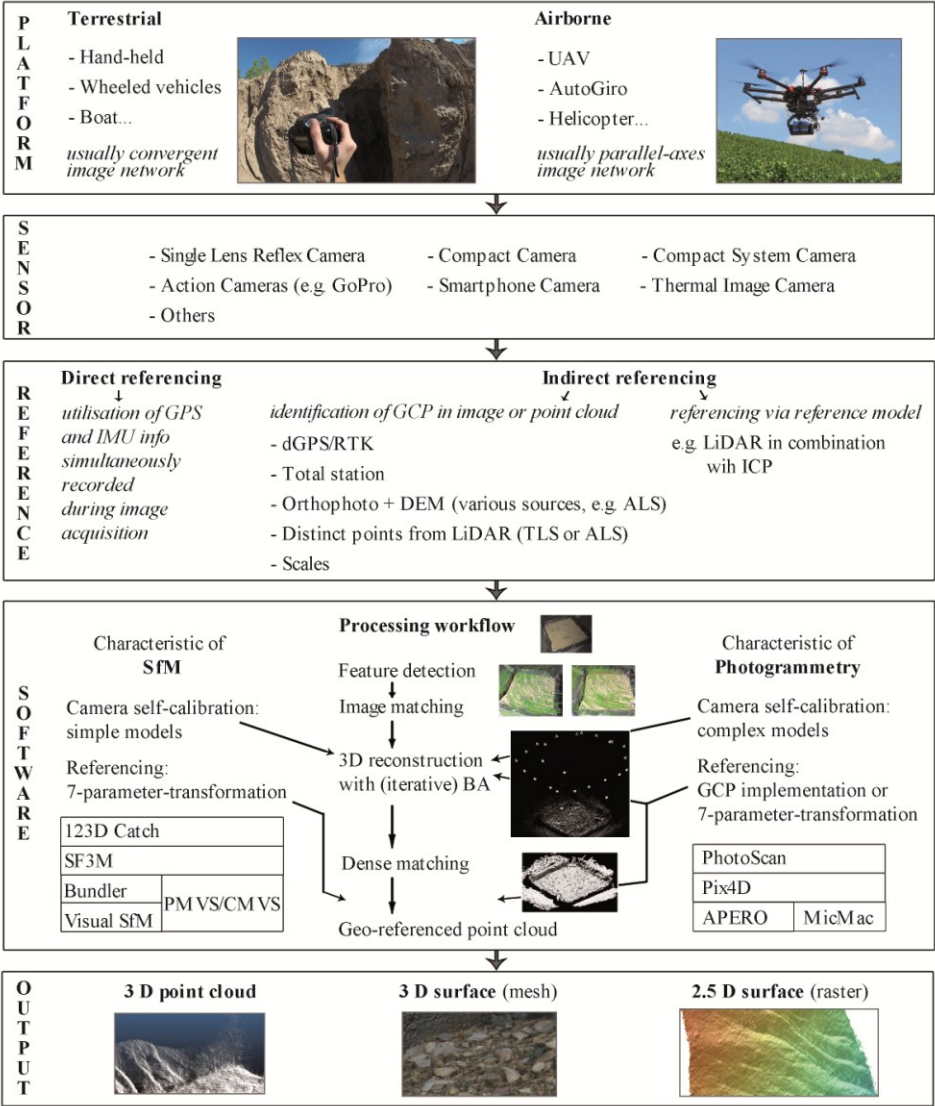
1628

1629 Figure 5. Performance of several error parameters in regard to the camera to surface
1630 distance. a) Characteristics of measured error and relative error (N: 54; ID 1-3, 5-12 and 14-39
1631 in Appendix A) . For grey coloured points GCPs are measured in point cloud (in total 9 times
1632 corresponding to the studies: ID 8, 11, 12, 28, 36, 37 in Appendix A) and for white points
1633 GCPs are measured in images (corresponding to the remaining studies) for model
1634 transformation. b) Superiority of the reference data (N: 33), which is calculated as ratio
1635 between measured error and error of the reference. Area based (ID 5-7, 12, 15, 17, 22, 25, 26,
1636 30 and 32 in Appendix A) and point based (ID 2, 3, 8, 9, 20, 24, 28-30, 33, 35 and 37 in
1637 Appendix A) reference measurements are distinguished. c) Theoretical error ratio, considering
1638 the theoretical and measured error, to illustrate SfM photogrammetry performance in field
1639 applications (N: 23; ID 1-3, 8, 10-12, 15, 21, 22, 25, 26, 28-30 and 32 in Appendix A).

1640

1641

1642 Figure 1:



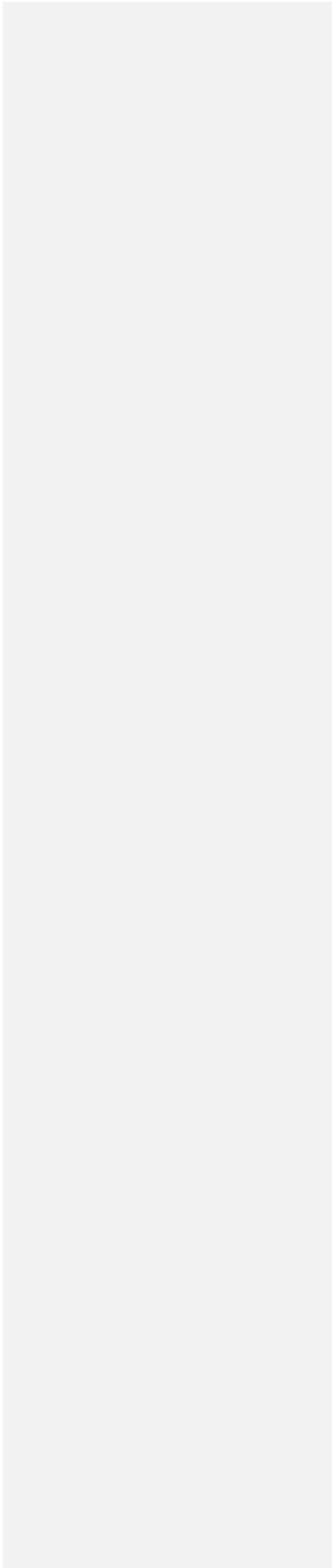
1643

1644

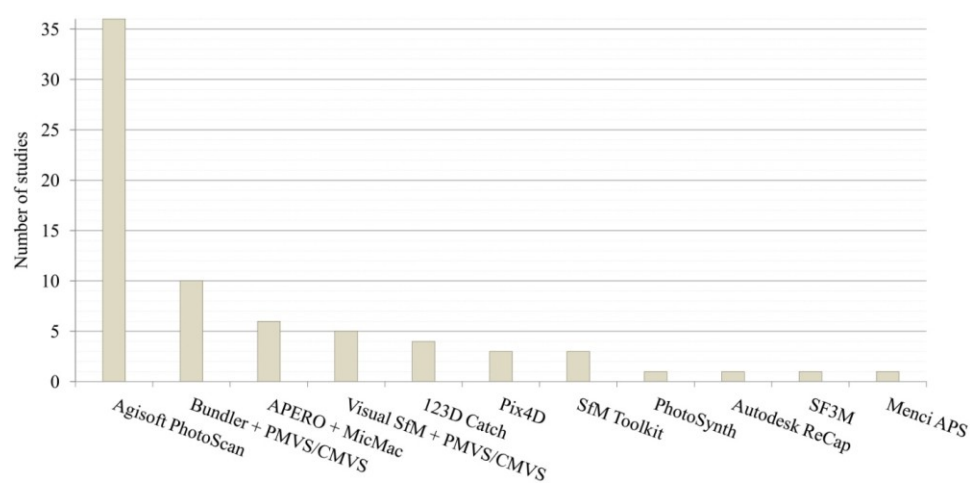
1645 Figure 2:



1646
1647



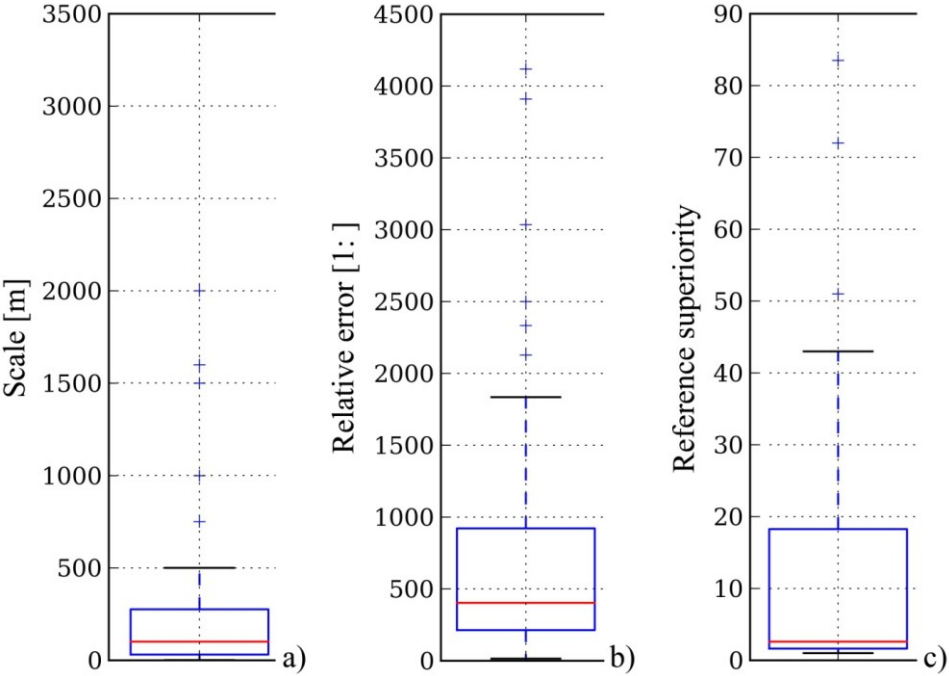
1648 Figure 3:



1649

1650

Figure 4:



1654 Figure 5:

